Frozen flux violation, electron demagnetization and magnetic reconnection

J. D. Scudder, H. Karimabadi, W. Daughton, and V. Roytershteyn

Citation: Physics of Plasmas **22**, 101204 (2015); doi: 10.1063/1.4932332
View online: http://dx.doi.org/10.1063/1.4932332
View Table of Contents: http://scitation.aip.org/content/aip/journal/pop/22/10?ver=pdfcov
Published by the AIP Publishing

Frozen flux violation, electron demagnetization and magnetic reconnection

J. D. Scudder,[1] H. Karimabadi,[2] W. Daughton,[3] and V. Roytershteyn[2]
[1]*Department of Physics and Astronomy, University of Iowa, Iowa City, Iowa 52242, USA*
[2]*SciberQuest, Del Mar, California 92014, USA*
[3]*Los Alamos National Lab, Los Alamos, New Mexico 87544, USA*

(Received 25 January 2015; accepted 22 April 2015; published online 6 October 2015)

We argue that the analogue in collisionless plasma of the collisional diffusion region of magnetic reconnection is properly defined in terms of the demagnetization of the plasma electrons that enable "frozen flux" slippage to occur. This condition differs from the violation of the "frozen-in" condition, which only implies that two fluid effects are involved, rather than the necessary slippage of magnetic flux as viewed in the electron frame. Using 2D Particle In Cell (PIC) simulations, this approach properly finds the saddle point region of the flux function. Our demagnetization conditions are the *dimensionless* guiding center approximation expansion parameters for electrons which we show are *observable* and determined *locally* by the ratio of non-ideal electric to magnetic field strengths. Proxies for frozen flux slippage are developed that (a) are measurable on a single spacecraft, (b) are dimensionless with theoretically justified threshold values of significance, and (c) are shown in 2D simulations to recover distinctions *theoretically* possible with the (unmeasurable) flux function. A new potentially observable *dimensionless* frozen flux rate, Λ_Φ, differentiates significant from anecdotal frozen flux slippage. A *single spacecraft observable*, Υ, is shown with PIC simulations to be essentially proportional to the *unobservable* local Maxwell frozen flux rate. This relationship theoretically establishes electron demagnetization in 3D as the general cause of frozen flux slippage. In simple 2D cases with an isolated central diffusion region surrounded by separatrices, these diagnostics uniquely identify the traditional diffusion region (without confusing it with the two fluid "ion-diffusion" region) and clarify the role of the separatrices where frozen flux violations do occur but are not substantial. In the more complicated guide and asymmetric 2D cases, substantial flux slippage regions extend out along, but inside of, the preferred separatrices, demonstrating that $\Lambda_\Phi \neq 0$ violations are present over significant distances (in ion inertial units) from the separator identified by the 2D flux function; these violations are, however, generally weaker than seen at known separators in 2D simulations.
[http://dx.doi.org/10.1063/1.4932332]

I. INTRODUCTION

This paper addresses the diagnosis of plasma and field signatures at possible space plasma sites of collisionless magnetic reconnection when flux functions, vector potentials, $\nabla \times \mathbf{E}_{||}$, and $J_{||}$ are *not* experimentally available during the spacecraft's transit time of anticipated electron inertial scaled current channels. This regime is the general circumstance for NASA's present space plasma experiments, including those recently launched on the Magnetospheric Multi-Scale (MMS) mission focused on the physics of collisionless magnetic reconnection.

In this situation, the identification of sites where magnetic reconnection is surely underway is non-trivial. To undertake this challenge, we have used Particle In Cell (PIC) simulations of magnetic reconnection in 2D where flux functions do exist within the code; there, we ascertain what *observable* signatures can be found within layers that are *known* to be reconnecting. This is clearly a learning process for the exploration phase that really takes place on such space missions where the potentially reconnecting sites are three dimensional and the first order question is the location of reconnection sites in the time records.

This paper emphasizes unique, observable dimensionless signatures that attend magnetic reconnection that can be anticipated by focusing on electron properties; of particular interest are those unusual attributes of the reconnection layers not known to be properties of otherwise well known normal modes or discontinuities in a plasma. We focus on those observable signatures that demonstrate that the sampled electrons have had their guiding center ordering disrupted. These new observables (and their derivations) demonstrate the central role that demagnetized electrons play in making collisionless magnetic reconnection possible. In addition, these electron properties reflect the relative sizes of the non-ideal electric and magnetic field in the layers, which in turn calibrate the strength of the non-ideal violations necessary to enable collisionless magnetic reconnection to occur. This insight provides a strong argument that reconnection sites cannot be identified by the mere non-zero size of the non-ideal electric field, which until now is commonly done.

Thus, the most selective identification of reconnection sites in space must proceed by screening event candidates for necessary, observable, properties of reconnection that are simultaneously rare in plasma physics at large. We will

demonstrate in this paper that the detection of electron demagnetization is such a screen, though imperfect. Various arguments will be presented that the agyrotropy of the electron plasma is essentially a measurement of the frozen flux violation. For the same reason that frozen flux violations need not imply the reconnection site, even such a rare indicator as this is still only a better screen for possible reconnection sites, not the invertible attribute for the reconnection site.

In loose terms, magnetic reconnection is made possible by a necessary "diffusion" region where "physics beyond Alfvén's ideal MHD" facilitates a steep, but smooth, transition between asymptotically sheared magnetic fields that are strongly compressed. Theoretically, the description can be made more precise, but at the expense of verifying conditions that are even difficult to perform within 3D simulations, let alone possible on the most advanced experiments flown on spacecraft. The vagueness of the first sentence explains the lack of consensus for what *observable* properties such a diffusion or transition region might possess. The wide inventory of phenomena offered in the experimental space literature as evidence that the reconnection has been witnessed or that the diffusion region has been transited is a further corollary of this imprecision. However, even in 2D simulations, where a flux function can be defined, numerous different operational suggestions have been made for what is the extent of the diffusion region in such idealized geometries.

Alfvén's idealization of "frozen-in" flow simplified the electrically conducting plasma description to the point where the lines of magnetic force could be profitably viewed as advected with the electron fluid's motion across the magnetic field. For this observer, the magnetic flux $\Phi = \int_C \mathbf{B} \cdot d\mathbf{a}$ threading a loop C, moving with this observer is conserved. This situation is *an example* of a "frozen flux" regime. In this regime, the "electron observer" (traveling with the electron fluid) observes magnetic field lines at rest: $\frac{d}{dt} \equiv 0$. The process of magnetic reconnection requires sharp and strong currents contrary to Alfvén's assumed currents that were broad and weak. For the electron observer near the diffusion region, Alfvén's approximations are unwarranted and the threading magnetic flux is no longer preserved. This is the regime of *"frozen-flux violation."* For the electron observer, Maxwell's equations determine the time rate of change of magnetic flux, ν_Φ, to be controlled by the comoving *total* rate of magnetic flux Φ evolution in the electron fluid's rest frame

$$\nu_\Phi \equiv \frac{d\ln\Phi}{dt} = -\frac{c}{\langle B\rangle A}\oint\int_C \nabla \times \mathbf{R}_e \cdot \hat{\mathbf{b}}\, da, \qquad (1)$$

where $\mathbf{R}_e = \mathbf{E} + \frac{\mathbf{U}_e}{c} \times \mathbf{B}$ is the *non-ideal* electric field Alfvén assumed to vanish, $\langle B\rangle$ is the average field strength projected on $\hat{\mathbf{a}}$ and A is the area of the closed curve C. The most general circumstance where magnetic flux is frozen (time independent) occurs whenever $\nabla \times \mathbf{R}_e = 0$, a circumstance that includes Alfvén's frozen-in regime as a special case (cf. Figure 2). Sometimes, this frozen-flux regime is referred to as the "no-slip" or "ideal" regime (cf. right hand side Figure 2) where a field line velocity can in principle be defined, although not generally given by $\mathbf{E} \times \mathbf{B}$. If the magnetic flux recorded by the electron observer evolves with time, this is the "slip" regime of non-ideal MHD where Maxwell's equations determine the comoving rate ν_Φ of this *frozen flux slippage* (cf. Eq. (1)).

Since reconnection in 3D is so complicated, considerable work has addressed reconnection in the 2D geometry where the possibility of a magnetic flux function (which is the out of plane component of the vector potential) simplifies, but constrains, the type of reconnection that is possible. Within 2D, the electron observer's comoving total time rate of change of the flux function, A_z (and hence the in-plane magnetic field components that determine the topology) is given by

$$\left.\frac{dA_z}{dt}\right|_{U_e} = -cR_{ez}. \qquad (2)$$

A curiosity of 2D geometries is that only the z component of the violation of Alfvén's frozen-in condition sets the time rate of change of A_z and hence the reconnection rate.

In 2D, the immediate vicinity of the saddle point of the flux function has historically been associated with the Electron Diffusion Region (EDR); the precise lateral extent of the EDR is the subject of ongoing debate. The 2D simulations shown below suggest that frozen flux violations occur many ion inertial lengths down the separatrices, away from the saddle point; however, these extended violations are comparatively weak. In 2D, there is a finite region, however, including the saddle point of the vector potential, where the frozen flux violations are "significant," so that such a region becomes a place where frozen flux violations are important and observable from their impact on the electron fluid's dynamics. These finite regions appear to be the analogue in collisionless 2D reconnection of the collisional EDR. We will refer to that region as the EDR in this paper. In subsequent papers in this series, we show that the additional freedom of 3D dynamics allows a more complicated evolution of the regions, where electron dynamics is modified by frozen flux violations, emitting flux ropes, and generating daughter sites for reconnection that vacate the idea that such a region for the full 3D geometry needs to remain simply connected. Thus, despite our usage of EDR in this 2D discussion, we suggest it is unlikely that a single EDR, rather than a "web" of EDR's will suffice for the actual 3D situation.

Using the generalized Ohm's law,[1] Vasyliunas showed[2] that the z component of the non-ideal electric field (in Eq. (2)) in 2D could only be supported at the separator if the electron pressure tensor was no longer well approximated by the cylindrically symmetric form $P_{ij} = P_\parallel \hat{b}_i\hat{b}_j + P_\perp(\delta_{ij} - \hat{b}_i\hat{b}_j) + \mathcal{X}_{ij}$, where $\hat{\mathbf{b}}$ is a unit vector along the local magnetic field direction, δ_{ij} is the unit tensor, and $\mathcal{X}_{ij} = 0$. Thus, Vasyliunas established that reconnection at the separator in 2D required the electron pressure tensor to contain a non-trivial cylindrical symmetry breaking part $\mathcal{X}_{ij}$. We refer below to the disruption of the pressure tensor that requires $\mathcal{X}_{ij}$ as the signature of *demagnetization* of the electrons.[3] When $\mathcal{X}_{ij}$ is not present,

the individual electrons in the plasma could be well modeled with a *gyrotropic* distribution function, cylindrically symmetric about the local magnetic field. In the presence of $\mathcal{X}_{ij}$, such distributions become agyrotropic distributions (with nontrivial velocity space dependence on v, θ_v and ϕ_v). Vasyliunas' deduction that demagnetized (agyrotropic) electrons are required near the separator in 2D has been fully documented by numerous independent PIC simulations.[4,13]

The usual theoretical justification for neglecting the $\mathcal{X}_{ij}$ parts of P_{ij} is the guiding center approximation.[3,5] This theory assumes weak gradients and slow time variations, predicting $\mathcal{X}_{ij}$ varies quadratically in the small perturbation parameters of the theory,[3] and hence is negligibly small if those expansion variables are small. This theory and the expectation that the first adiabatic invariant μ should be conserved are the basis of common expectations that plasmas should be magnetized with $\mathcal{X}_{ij} \simeq 0$. Specifically, the expansion variables for each species involve dimensionless ratios like gyroradius over scale length or time scale compared to the gyro period.

Vasyliunas' conclusion implied that the guiding center approximation cannot be an accurate description of the electrons in the plasma near the separator in 2D. Below, we refer to this result as *Vasyliunas' theorem*. With $\mathcal{X}_{ij}$ nonnegligible, it is logical to associate the incidence of strong gradients that contradict the assumptions of guiding center approximation with the layers attending collisionless reconnection as seen in full PIC simulations.[6,7] In this sense, demagnetization of the electrons is viewed as a necessary condition for the frozen flux violation required for 2D reconnection.

In understanding the circumstances where electrons become demagnetized, we have been able to generalize Vasyliunas' suggestion to 3D geometries of reconnection, motivating that the frozen-flux slippage rate there is proportional to the dimensionless indices of demagnetization that characterize the importance of $\mathcal{X}_{ij}$ for the pressure tensor.[7] Unlike the 2D limitation of flux functions, our guiding center approximation based arguments are not restricted to two dimensions. The guiding center approximation assumes that three quantities are small for each species in the plasma: $\{\delta_j, \epsilon_j, \tau_j\} \ll 1$, which correspond to assuming that the specie's thermal gyroradius is small compared to gradient scales, the energy gain per cyclotron period is small compared to kT_j, and the frequencies encountered are slow compared to Ω_j, the cyclotron frequency, respectively. Below, we show that these parameters are *local* and interrelated and that the first two are routinely *measurable* by a single spacecraft using already flown space plasma instrumentation or by local operations in a PIC simulation.

Our proxy analysis in this paper determines all of these expansion parameters from PIC simulations of magnetic reconnection, demonstrating that these quantities are nonuniformly enhanced within the reconnection current channel whose locations are established with the flux functions that exist for these 2D simulations. These signatures are shown to be non-perturbative in the PIC layers that form self consistently and hence represent observable proxies for demagnetization and hence frozen-flux violations. These parameters are indicated by the red rows in Figure 1.

The predicted parameter regimes of electron demagnetization foreseen for the reconnection current layer are well removed from the typical properties of the ideal MHD plasma; furthermore, these properties are not those of other plasma phenomena. Thus in both 2 and 3 dimensions, there is clear theoretical motivation that observable evidence for frozen flux violation may be provided by searching for evidence of demagnetization of the thermal electrons.

The thresholdless nature of non-zero demagnetization, $\delta_e \simeq \rho_e/L > 0$, or frozen flux violations, $\nu_\Phi \neq 0$, leads to the perplexing situation that not all such sites are reconnection layers. We show clear evidence for this conundrum along separatrices where both quantities are non-zero. To eliminate this source of confusion, we have studied and developed ways to rescale the rate of frozen flux violation into a dimensionless quantity, Λ_Φ (cf. Figures 1–3), so "significant" violations, $\nu_\Phi \neq 0$, may be quantitatively separated from "anecdotal" slippages that occur at the separatrices in 2D, or in other narrow electron inertial scaled channels where reconnection may be geometrically forbidden (cf. Section VI C).

While Maxwell's rate of frozen-flux violation ν_Φ is not a direct observable, we show below that

$$\nu_\Phi \sim \Upsilon = \Omega_{ce}\delta_e^2 \tag{3}$$

is an observable proxy for frozen flux slippage (cf. Figure 1).

Observable local corollaries of electron inertial scaled current channels suggest additional dimensionless proxies

Quantity	Name	Expectation	Observable?	Defining Equation
$\frac{dA_z}{dt}$	Change of Flux Function (2D)	$\neq 0$	No	I-2
ν_Φ	Frozen Flux Change (3D)	$\neq 0$	No	I-5
Υ	ν_Φ Proxy	$\simeq \nu_\Phi$	Yes	I-3
δ_e	Demagnetization	$O(1)$	Yes	I-8
ϵ_e	Energy Change	$O(1)$	Yes	I-12
τ_e	Frequencies Present	$O(1)$	Perhaps	I-20
M_e	Electron Thermal Mach Number	$O(1)$	Yes	I-13
$A\emptyset_e$	Agyrotropy	$O(\delta_e^2)$	Yes	I-22
α_e	Angle $\hat{\mathbf{E}}_\perp$ and Eigenvectors of $\mathbf{P}_e$	$<< 20^o$	Yes	I-23
$\frac{\partial E_n}{\partial n} < 0$	Convergent Electrostatic	$200\mu V/m$	Yes	I-24
$\Lambda_{e,\Phi,\uparrow}$	Dimensionless $\nu_{e,\Phi,\uparrow}$	$O(1)$	No	I-7

FIG. 1. Index of proxies: Red grid contains observable proxies that reflect violations of the premises of guiding center approximation; some of these proxies δ, ϵ, τ are the assumed small expansion parameters of guiding center approximation theory. When they are not small compared to unity, the electrons are demagnetized. Λ is a dimensionless form of frozen-flux violation that when larger than one suggests frozen flux slippage is dynamically important. *The precise functional scaling of these expectations with guide field strength is not known theoretically. Some evidence for this variation is shown in Section VII D.*

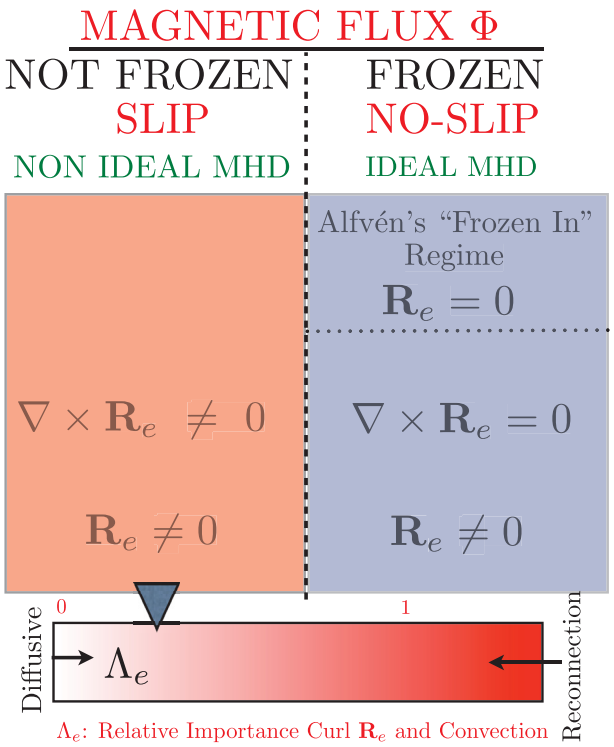

FIG. 2. Contrast of the non-ideal MHD condition, $\nabla \times \mathbf{R}_e \neq 0$ (top-left), from the ideal MHD, $\nabla \times \mathbf{R}_e \equiv 0$ (top-right), based on the size of $\nabla \times \mathbf{R}_e \neq$, $= 0$. Alfvén's "frozen-in" regime is only a *subclass* of ideal MHD. Horizontal bar (bottom) denotes the role of proposed index Λ_e, a scaled version of $\nabla \times \mathbf{R}_e$, proposed in this paper to differentiate degrees of violation of frozen flux: varying from weak, termed "diffusive," to very strong $\gg 1$ that is necessary for the usual layers that attend magnetic reconnection.

for sites of electron demagnetization that form the rows 7–10 of Figure 1. The first involves the electron thermal Mach number, M_e, required to satisfy Ampére's equation, which should be order unity; the second involves the observable experimental inventory of the departure from gyrotropy of the electron pressure tensor; this *agyrotropy*, $A\emptyset_e$, should scale like δ_e^2.

Fig. 1 represents a number of interlocking proxies for inferring the size of the assumed small dimensionless parameters of guiding center approximation that predict the gyrotropic $\mathcal{X}_{ij} \simeq 0$ simplification of the pressure tensor and forestall collisionless reconnection. *Most of these relations have an unknown multiplying function of guide field strength, which is not currently known. The expectations placed in this table are for weak guide fields, comparable to the reconnecting field. Some indications of behavior with guide field strength are shown in Section VII D.* Falsifying any of these proxies vacates the expectation that the pressure tensor is gyrotropic. While these conditions are functionally related, some are more accessible to measurement than others, or need different mixes of independent observables to construct. As an ensemble, they can offer mutual reinforcement when attempting to identify the diffusion region in 3D space observations. Quite apart from the reconnection problem, these proxies provide a natural way to "see" the incidence of narrow electron scale physics in large scale simulations, or to look for this evidence in *in situ* data with applications for turbulence in the dissipation range.

After Section I, this paper is organized in the following sections: II. Concepts and Descriptions of Reconnection; III. New Tools for Diagnosing Reconnection in 3D; IV. Frozen Flux Slippage via ν_Φ or $\frac{d\ln A_z}{dt}$; V. Measurable Scalar Proxies for Electron Demagnetization; VI. Flux Slippage, Flux Function, and Demagnetization in 2D; VII. Demagnetization and Flux Slippage: 2D Guide Geometry; VIII. 2D Asymmetric Signatures of Demagnetization; followed by Discussion and Summary in Section IX.

II. CONCEPTS AND DESCRIPTIONS OF RECONNECTION

When magnetic reconnection occurs, bundles of magnetic flux passing through a "sufficiently cohesive" non-ideal region ($\nu_\Phi \neq 0$) no longer have global equations of motion and a change of magnetic topology is usually involved; neither a *non-ideal region* nor a *change of magnetic topology* is concept with readily observable signatures. The experimental searches in nature for objective evidence for magnetic reconnection contain semantic tangles as observers' chain perceptions of the process with imprecisely specified targets of their study. Some of these connections are "borrowed" from theoretical arguments of geometrically simplified (2D) descriptions of reconnection that do *not* generalize to the three dimensional situations where evidence for reconnection is sought.

One of the objectives of this paper is to introduce physically motivated lower bounds, or thresholds, for the ≥ 0 conditions of Figures 2 and 3 so that detections exceeding such thresholds have a much increased likelihood to be about magnetic reconnection than about more common processes or, even, measurement error. As we shall see, conditions of

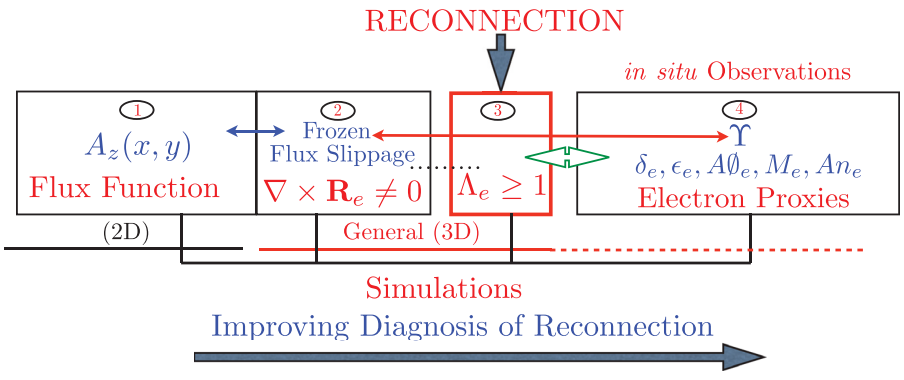

FIG. 3. Progression of the paper from 2D specific diagnosis to those for 3D, showing relation between tools for measuring flux slippage [ν_Φ, Υ], dimensionless slippage, Λ_e, and electron specific observable proxies for the electron diffusion region.

the form $Y=0$, such as Alfvén's approximation, are extreme idealizations that invariably have weakly non-zero violations. We must then formulate conditions for reconnection that involve dimensionless quantities.

We lay out an argument connecting the process of collisionless magnetic reconnection and the occurrence of current layers so thin that the thermal electron gyration about the magnetic field is disrupted, that is, the thermal electrons are *demagnetized*.

There are several well known ways that such demagnetization can be produced, and by implication one or all of these circumstances must be surveyed for these possibilities. We formulate *dimensionless, but observable indices* of electron demagnetization, and show with full particle simulations that they are actually sizable within layers where collisionless magnetic reconnection is known to be underway.

A necessary property of this type for the reconnection layer is that there frozen flux slippage must occur: $\nu_\Phi \neq 0$. For there to be such slippage, the curl of the non-ideal electric field, $\mathbf{R}_e \equiv \mathbf{E}+\mathbf{U_e}\times\mathbf{B}/c$, must be non-vanishing (so that $\mathbf{R}_e \neq 0$ is also required). This approach leads to terming the reconnection layer as a product of the "non-ideal" regime (which it is with $\mathbf{R}_e \neq 0$), and that it can be found by finding violations of Alfvén's "*ideal MHD*" approximation *which it cannot*. Many violations of Alfvén's ideal MHD approximation are pedestrian frozen flux regimes where $\nabla\times\mathbf{R}_e=0$.

The key property of non-ideal regions is that they are locales where magnetic flux is not stationary in the electron fluid's frame of reference; this situation is also said to be where the "frozen-flux" circumstance is violated. The most general ideal MHD regime is one where the "frozen-flux" condition, $\nabla\times\mathbf{R}_e=0$, obtains. It is a more general regime than that proposed by Alfvén (cf. right hand side Figure 2) since his ideal MHD achieved a restricted form of frozen flux conservation by positing that a truncated form of the generalized Ohm's law, $\mathbf{R_e}\equiv\mathbf{E}+\mathbf{U_e}\times\mathbf{B}/c\simeq 0$, would often be a good approximation for astrophysical plasmas. Alfvén's $R_e\equiv 0$ regime is referred in the literature as the "frozen-in" regime, and with its spatially invariant size ensures the frozen-flux condition follows, since then $\nabla\times\mathbf{R}_e=\nu_\Phi\equiv 0$. In spite of this progression, the logic is of the *if then* form and not of the *if and only if* form. *Alfvén's frozen in approximation* and his ideal MHD achieves a restricted enforcement of *frozen-flux* that more generally occurs whenever $\nabla\times\mathbf{R}_e\equiv 0$ which occurs in all blue shaded regions in Figure 2.

The confusion comes when it is realized that there are other ways with $\mathbf{R}_e\neq 0$ and $\nabla\times\mathbf{R}_e\equiv 0$ to achieve *frozen-flux* that do not require *Alfvén's frozen-in* assumption (lower half of blue shading of Figure 2). *Thus, to detect a non-ideal regime where frozen-flux is violated, it is insufficient to demonstrate a violation of Alfvén's frozen-in approximation*. (A simple example involving $\mathbf{R_e}\equiv\mathbf{E}+\mathbf{U}_e\times\mathbf{B}/c\simeq-\frac{\nabla P_e}{en_e}$ will have a vanishing curl although $\mathbf{R}_e\neq 0$, whenever the electron pressure is only a function of the local density - as with polytropic closure.)

Nonetheless, arguments are common in the literature, which rely on demonstration of $\mathbf{R}_e\neq 0$ to identify a current channel as a non-ideal site where frozen flux "violation" has been observed. Perhaps, a part of this confusion results from the situation in 2D where only the out of plane violations of Alfvén's frozen in condition actually imply reconnection (cf. Eq. (2)). Thus, even in 2D, there are circumstances where Alfvén's "frozen-in" condition may be violated and there is still no reconnection implied! The overarching *necessary* condition for reconnection is that frozen flux must be violated. Certifying frozen flux violation in the 3D circumstances of space requires something beyond establishing $\mathbf{R}_e\neq 0$.

All conditions in the blue shaded portion of Figure 2 are consistent with the *"frozen in" ideal MHD* approximation, also known as the *no-slip* condition, in which the equation of motion for magnetic field lines is the same as the components of the electron bulk motion transverse to the magnetic field. In this regime, the magnetic field is passively advected by the electron center of mass flow's components transverse to **B**. The opposite *non-ideal*, or *slip*, regime of MHD where $\nabla\times\mathbf{R}_e\neq 0$ occurs in the left, red shaded, half of Figure 2. In these regimes, there are no equations of motion for flux tubes, and the idealization of frozen flux advected by the electrons, is no longer a rigorous "short-hand" for the plasma's behavior. In this regime, a more complete physical theory based on the time and space evolution of the four vector potential is required to predict the temporal evolution of the system.

However, the condition for frozen flux violation (Eq. (1)) is an example of a condition without a threshold. Does reconnection ensue regardless of the non-zero size of ν_Φ? An interesting question we will try to answer is how much slippage is sufficient to suggest that frozen-flux enabling dynamics, like magnetic reconnection, has been witnessed? While all such regions are non-ideal, the detection of frozen flux violations $\nabla\times\mathbf{R_e}\neq 0$ in any given locale does not lead inexorably to the conclusion that one is near the topology changing layers.

From the one fluid equation for the plasma, Alfvén's idealization is equivalent to ignoring currents, pressure gradients, and accelerations. In this *Alfvén ideal MHD* regime, where $\mathbf{J}_\perp\simeq 0$, the magnetic flux is equally well described as frozen in the electron's frame of reference, since the transverse components of the center of mass velocity and that of the electrons or protons (where both species are magnetized) are the same. However, in the presence of gradients of scale L, the magnetic flux can be described as "frozen in" to the electron's frame down to much shorter scales than if attempted in the ion or the center of mass frame.[1] As the system develops still narrower layers, it can approach the larger of the electron's skin depth or gyroradius; in this regime and in the appropriate geometries, the visualization of the advection of the magnetic field by the electrons becomes less faithful and the domain of flux slippage (top left in 2) in the electron frame is *potentially* at hand, as is the possibility for magnetic reconnection. Such regimes are certainly *non-ideal* according to most authors.

The violation of the frozen flux idealization[1,8] for the total comoving $\frac{d}{dt}$, evolution of the magnetic flux, Eq. (3) can be rewritten in the spirit of the mean value theorem as

$$\frac{d\langle B\rangle}{dt} = -c\langle \hat{\mathbf{b}} \cdot \nabla \times \mathbf{R}_e \rangle, \tag{4}$$

where $\langle\,.\,\rangle$ denotes an average over a small, but non-zero area bounded by the closed curve C. The time scale for the violation of frozen flux is determined by the *spatial variation* of the non-zero properties of the *non-ideal electric field*. A measure of the experimental difficulties in assessing this rate comes into focus when it is realized that it involves the curl of an electric field that is zero in leading order, and is thus even more difficult to measure than the electric field itself, which has only recently become quasi-routine.

From Eq. (4), we can estimate a local loop average for time scale τ_Φ for *flux slippage* to be

$$\nu_\Phi \equiv \frac{1}{\tau_\Phi} = \frac{d\ln\Phi}{dt} = -\frac{c\langle \hat{\mathbf{b}} \cdot \nabla \times \mathbf{R}_e \rangle}{\langle B\rangle}, \tag{5}$$

showing explicitly the sense in which this rate is determined by the curl of the non-ideal electric field.

Similar considerations using the cross, rather than the dot, product in Eq. (3) lead to estimates for the time scale $\tau_\uparrow$ for violations of *magnetic line preservation*[9] that have a frequency and time scale estimates of the form

$$\nu_\uparrow \equiv \frac{1}{\tau_\uparrow} = \frac{d\ln\Phi_\uparrow}{dt} = -\frac{c\langle \hat{\mathbf{b}} \times \nabla \times \mathbf{R}_e \rangle}{\langle B\rangle}. \tag{6}$$

Flux slippage is said to occur when the number of lines of force per unit area, that is the magnetic flux Φ through the area C, is not preserved as C is deformed with the observer's $\mathbf{U}_e(x, y, z, t)$. The rate of *line slippage*, denoted as $\nu_\uparrow$, refers to the absence of the preservation of labeled lines of force per unit area contributing to the flux through the moving curve C. Since line violation is the stricter condition, it will be violated more frequently than flux preservation; thus, it should generally be expected that $\nu_\uparrow \geq \nu_\Phi$ in the same locale, which we have shown statistically.[7] However, there do appear to be regimes in PIC simulations where either of these violations takes precedence.

III. NEW TOOLS FOR DIAGNOSING RECONNECTION IN 3D

Our overall program in this paper is schematically indicated in the panels of Figure 3. First, we show that the curl approach can obtain the rates of frozen flux violation determined in 2D using the total time variation of the flux function (insets 1, 2). Second, we show that our five scalar tools properly identify the regions that would be called the diffusion regions in 2D simulations based on the flux function. Third, we seek to establish the relationship of these indices of electron demagnetization with those where flux slippage is seen in 3D reconnection to see if they provide insight, in the absence of flux functions, where reconnection is underway (insets 2–4).[7]

A. Time scales for flux slippage vs fluid motion: Λ_e proxy

We now briefly discuss at the overview level the two major ways that we will suggest yardsticks to make our measures of the reconnection site dimensionless.

Because the site(s) of flux slippage occur in narrow current channels, the effectiveness of flux slippage in the system's evolution should involve the comparison of electron time scales to transit the slippage, $\tau_{\mathbf{U}_e}$, and the (co-moving) intrinsic time scale of the flux slippage process, τ_Φ. Our suggestion for introducing significance of flux slippage is through this ratio of time scales, defining

$$\Lambda_\Phi \equiv \frac{\tau_{\mathbf{U}_{e,\Phi}}}{\tau_\Phi} = \frac{\nu_\Phi}{|\mathbf{U}_e \cdot \nabla \ln \nu_\Phi|}, \tag{7}$$

where ν_Φ denotes the rate of flux violation. Analogous quantities $\Lambda_\uparrow$ can be constructed for rates and times to traverse line variations. When not differentiating between line or flux versions of Λ, we will use the symbol Λ_e.

Λ_e *can be very small*, as in a shock layer, whenever the time scale of electron transit of the flux slippage region is shorter than the time scale of flux slippage. Clearly, small $\Lambda_e \ll 1$ layers can still possess *"diffusive"* non-zero flux violations, they just have an insignificant impact on the large scale evolution of the hydromagnetics. Conversely, the developed quasi-steady models of reconnection invariably involve matching the electron hydrodynamic time scale for replenishment of magnetic flux with the time scale for its slippage/erosion, which is similar to the suggesting that such regimes should have $\Lambda_e \sim 1$. We show below with PIC simulations in Figures 5(b) and 6(e) that this type of dimensionless scalar does a good job of finding the locales in 2D simulations, where the reconnection takes place *which flux functions can verify* and where the electron proxies of demagnetization, made dimensionless, are usually sizable. In Section VI C, we also demonstrate that Λ_e is well calibrated.

B. Electrons demagnetization and corollaries: Five scalar proxies

If demagnetization of electrons is central to collisionless magnetic reconnection, it can be recognized as the opposite regime from the more typically expected magnetized regime for plasmas. The guiding center approximation assumes for each species in the plasma that three dimensionless expansion parameters are small compared to unity.[3] These parameters for electrons, labeled here as $\{\delta_e, \epsilon_e, \tau_e\}$, correspond to (i) gyro radius divided by gradient scale; (ii) work done per gyro-period in kT_e units; and (iii) frequency of time variations scaled by the gyro period, respectively. An analogous set for the ions may be defined with obvious changes for mass, charge, and temperature. The onset of ion demagnetization suggests the penetration of two-fluid like layers in the plasma, such as occur in Hall MHD regimes. However, until the electrons are also demagnetized, such ion signatures have no direct implication concerning magnetic reconnection. This separated morphology can cause, but is not unique to, the "ion diffusion" region outside of the proper layer where magnetic flux and the electron flow become uncoupled.

The sizes of these electron guiding center expansion parameters are shown (below) to be proportional to the *dimensionless size* of the non-ideal electric field scaled by the magnetic field, $\frac{|\mathbf{R}_e|}{B}$, rather than the threshold-less non-zero

size of $|\mathbf{R_e}|$ alone. (Note that in Alfvén's frozen in regime, this ratio vanishes, showing its close connection to the perturbative underpinnings of MHD.) A given sized non-ideal electric field, $|\mathbf{R}_e|$, can be *demagnetizing* in weak B regimes, but consistent with *strong magnetization* in much stronger B regimes. This clarifies the confusing arguments that $|\mathbf{R_e}| \neq 0$ suffice to identify the region where the (electron) frozen flux theorem is violated.[10–12,15]

Accordingly, the way to find the demagnetized regions is to identify spatial regimes where *any* of these guiding center expansion parameters are order unity. Thus, our recipe for finding direct *observables* of theoretically direct measures of electron demagnetization becomes either $\{\delta_e \simeq O(1)\}$ and/or $\epsilon_e = O(1)$ or the implications of same as discussed below. This condition is so useful we define $\kappa_e(x, y, z) = max[\delta_e(x, y, z), \epsilon_e(x, y, z)]$, to compactly rephrase the conditions for demagnetization: $\kappa_e = O(1)$.

If $\kappa_e \ll 1$ is small in some region, the electrons are almost surely magnetized. Conversely, contiguous region where $\kappa_e = O(1)$ is clearly suitably categorized as demagnetized. *Any experimental use of* κ_e *must first baseline the calibration of the various instruments involved by showing generally that routine observations produce* $\delta_e \ll 1$ *and* $R_e \ll E$ *in regimes where MHD is expected to prevail.*

We have not discussed direct measures of τ_e since it is not presently known with space observations how to separate observed time variations into those explicitly associated with $\frac{\partial}{\partial t}$ versus advectively caused variations. Another potential complication as with wave particle interactions is the possibility that the time variations, as in resonant interactions, are only seen by a subset of the species, while non-resonant phenomena might perturb the distribution more widely. However, below we show that it is possible to locally estimate the rate of frozen flux violation through our new proxy parameter, Υ. *We emphasize below that* δ, ϵ, κ, *and* Υ *are direct observables possible with current state of the art instruments on already deployed spacecraft.*

Other observables may be determined with *less* effort than the guiding center approximation's perturbation variables themselves. Because the observables theoretically scale as simple functions of these variables, their measurement may infer the size of the expansion variables. The size of these additional *observables*, such as the electron fluid's thermal Mach number M_e is so unusual (cf. Figure 7(a)) that they can be thought of as either independent or corroborative measurements to the primary violations of the perturbation variables above. Among these variables described in detail in Section V E are $A\emptyset_e = O(1)$, $M_e = O(1)$, $An_e > 2 - 10$, $\angle(\mathbf{E}_\perp$, Eigenvectors of $\mathbf{P}_e) \ll 10^\circ$, involving agyrotropy, electron thermal mach number, electron anisotropy, and angle of attack of $\mathbf{E}_\perp$ on the pressure tensor, respectively.

IV. FROZEN FLUX SLIPPAGE VIA ν_Φ OR $\frac{dA_z}{dt}$

Since the flux function method is the standard in 2D for assessing rates of magnetic reconnection, we first establish with Figure 4 that the numerical rates of flux slippage in the form of $\nu_\uparrow$ derived from $\nabla \times \mathbf{R}_e$ are proportional to the traditional estimates based on $\frac{dA_z^{sp}}{dt}$, determined by the total time variation of A_z^{sp} at the evolving saddle point (sp). The simulation used was of symmetric anti-parallel geometry with $M/m = 400$ and $\frac{\omega_{pe}}{\Omega_{ce}} = 2$. The plot in Figure 4 connects coordinate pairs of estimates of $\left[\frac{dA_z^{sp}}{dt}|_{U_e}, \langle \nu_\uparrow \rangle\right]$ determined by a finite difference estimate using the flux function, and an average $\langle \nu_\uparrow \rangle$ of the estimates from the spatial curls at the saddle point at the two different times involved in the finite difference of the vector potential: $\left(\frac{\Delta A_z^{sp}}{\Delta t}|_{(1\to 2)}, \langle \nu_\uparrow \rangle\right)$, where the "X" point moves in time between $(x_1, y_1, t_1) \to (x_2, y_2, t_2)$. The red line in the figure is the best regression and is consistent with the ordinate and abscissa essentially equal, with the slight discrepancies attributable to the finite differences in A_z performed across simulation output frames, whereas the $\langle \nu_\uparrow \rangle$ were determined as a time average $\langle \nu_\uparrow \rangle = (\nu_\uparrow(x_1, y_1, z_1, t_1) + \nu_\uparrow(x_2, y_2, z_2, t_2))/2$. It should be noted that the finite differences in $\frac{dA_z}{dt}$ and errors of locating the saddle point (for comparisons) are important limits on the precision of the presented comparison as are the different noise characteristics of the curl operation for $\nu_\uparrow$ as contrasted with the very smooth form of the vector potential.

This comparison confirms the ability of the curl operations via $\nu_\uparrow$ to deduce the same information that the flux function can *only provide* in 2D. Thus, the approach for $\nu_\uparrow$ or ν_Φ clearly has the "same" information in 2D, but at present is the *only* known local approach for determining frozen flux slippage in 3D geometries.

A spatial map of $\log_{10}\nu_\uparrow$ across a $M/m = 400$, anti-parallel 2D PIC simulation[13] is shown in the top inset of Figure 5. The highest values of $\nu_\uparrow$ occur astride the same saddle point region indicated more simply (in this 2D simulation) from the white isocontours of A_z which play the role of flux function. The structure of the colored relief plot is determined only by the variations of $\nu_\uparrow$ determined from derivative operations, Eq. (6), using **B**, **E**, and $\mathbf{U}_e$ fields only. Superposed black contours in this figure reflect the

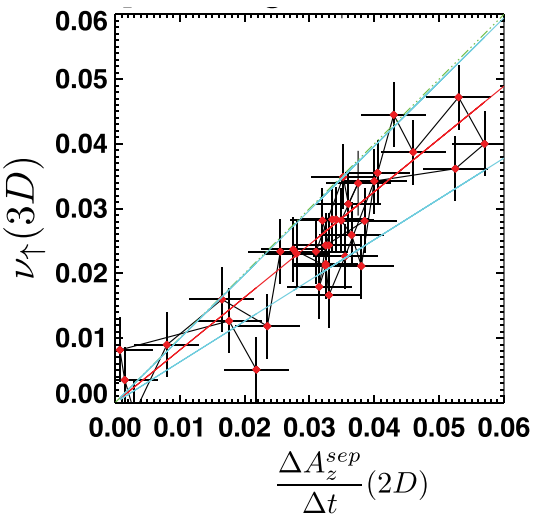

FIG. 4. Correlation over time between $\frac{\Delta A_z}{\Delta t}$, a 2D tool, and $\nu_\uparrow$, a tool valid in 3D. Estimates are red dots. At 95% confidence, best fit via hypothesis testing (red) with slope $m = 0.81 \pm 0.18$ is consistent with equality (green dashed line) of the two measures. Cyan lines suggest 95% confidence bounds on the linear regression.

topography of $\kappa_e = 1$, 0.3 (the "downhill" direction is indicated by the flags). The mesa of high κ_e readings also shows the same topography as $\nu_\uparrow$ and conforms to the saddle point topology of the vector potential. The regions of the most intense $\nu_\uparrow$ are enveloped by the nested contours of $\kappa_e = \{1, 0.3\}$, which represent our new, composite, dimensionless indicator of violations of the electron guiding center approximation. Figure 5 suggests the promise of the present *observable* proxy program (inset 4 in Figure 3) using $\kappa_e = O(1)$ to find the locally highest values of $\nu_\uparrow$, *without* the laborious curls required for $\nu_{\uparrow_e}$, not to mention the multi-spacecraft observations it would require, if it were even technically feasible.

However, a wide variation of non-zero $\nu_\uparrow$ occurs *throughout* the simulation plane in Figure 5(a). The variation of Λ_e discussed above and whose common logarithm is shown in Figure 5(b) answers the question: *where in this simulation is flux slippage "significant"?* The common black isocontours of $\kappa_e = 1{,}0.3$ across both (a) and (b) panels provide a clear reference between $\log_{10}\Lambda_e \geq 0$, enclosed by $\kappa_e \simeq O(1)$, where the electrons are clearly demagnetized. By this approach, Λ_e in the exhausts (near "C") is several orders of magnitude depressed relative to $\Lambda_e > 1$ near the saddle point region. The values of Λ_e are even smaller across the separatrices (near "B"), where $\nu_\uparrow$ is non-zero, but the time scale for the electron fluid to transit these layers is so short that the impact of such weak rates of $\nu_\uparrow$ is inconsequential to the description of the magnetized fluid. This technique also suggests inconsequentially low values of Λ_e in the inflow regions, consistent with their alternate signatures of being strongly magnetized, $\kappa_e \simeq 10^{-4}$.

Thus, we begin to have a picture of the *"significance" of flux slippage $\nu_\uparrow$ that depends on the competing dynamical context*: if the electrons flow rapidly, transiting the spatial gradients of the flux slippage more rapidly than the time scale of the slippage, the slippage can be rendered ineffective, even though the same rate of slippage with slower electron dynamics might be very significant.

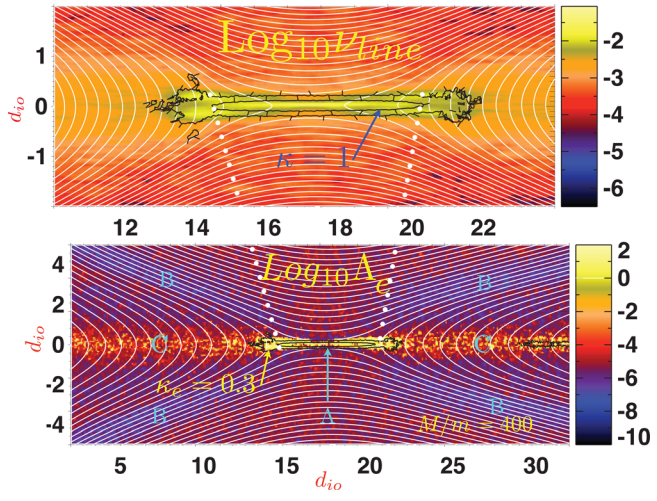

FIG. 5. (a) Variation of $\nu_\uparrow$ and (b) of $\log_{10}\Lambda_e$. Black contours in both panels are for levels of kinetic proxy for electron demagnetization, $\kappa_e = 1$, 0.3, with flags on contour indicating the "downhill" direction. These figures show that $\kappa_e \simeq O(1)$ provides a very accurate proxy for the indicators from Maxwell's equation that strong reconnection is underway, $\Lambda_e \gg 1$.

Figures 5(a) and 5(b) show that flux slippage is significant (via $\Lambda_e \geq 1$) across the main part of the saddle area and weakens out into the separatrices; strong competition of time scales caused by fast flows implies the rapidly reduced "significance" of the residual slippage on the separatrices as one moves away from the saddle point proper. This figure provides support for the progression in Figure 3 between "flux slippage" (inset 2) that requires $\nabla \times \mathbf{R}_e > 0$ and "significant flux slippage" that is indexed by $\Lambda_e = O(1)$ (inset 3) in the same current channel. This distinction is now possible with a scalar *dimensionless* Λ_e proxy for the necessary flux slippage for reconnection, and the knowledge that when larger than order unity the electron fluid dynamics is moderated by the flux slippage.

While Λ_e is of considerable theoretical interest, as here, for 2D numerical simulations, it may be of considerable use when theoretically diagnosing reconnection in 3D. However, as the ratio of two quantities that depend on partial derivatives, its determination from PIC is computationally intensive; a low noise variant is unlikely to be available soon from space plasma measurements because of the difficulty of determining an accurate $\nabla \times \mathbf{R}_e$ even using multiple spacecraft, followed by gradient operations on it to obtain the denominator of Λ_e. With this perspective and the demonstration above of the proxy property of $\kappa_e \iff \Lambda_e$, the *observable* κ_e diagnostic may be immediately useful as an approach to help locate frozen flux violations. These results also suggest that κ_e and $\Lambda_\uparrow$ variations may be helpful for finding flux slippage layers in 3D PIC simulations where there is no flux function.[7]

V. MEASURABLE, SCALAR PROXIES FOR ELECTRON DEMAGNETIZATION

The basic idea is to follow the implications of disruptions of the electron guiding center expansion variables, since if found they vacate expectations for cylindrical symmetry of the electron pressure. In this sense, for example, locales with non-negligible

$$\delta_e \simeq \frac{\rho_e}{L} \tag{8}$$

help to identify places where the electron fluid's capacity to "label" field lines would be compromised.[1,4] As we show below, when one of the expansion variables is large, the others are also sizable.

A. δ_j: Fluid frame perpendicular electric force is small relative to magnetic force

The physics of the small δ_j expansion is that the ratio of the average perpendicular electric to magnetic force felt on the jth species thermal speed $w_{\perp,j}$ particle with charge $q = |e|Z_j$, *as viewed in the frame of its bulk velocity*, $\boldsymbol{U}_j$, should be small.[3,14] Thus,

$$\delta_j = \frac{|Z_j(cE_\perp + \mathbf{U}_j \times \mathbf{B}|}{Z_j w_{\perp,j} B} \equiv \frac{c}{w_{\perp,j}} \frac{R_{j,\perp}}{B} \ll 1. \tag{9}$$

It is instructive to recover from $\delta_e \ll 1$ the frequently invoked summary of guiding center theory, that it is valid for

small gyroradius over scale length regimes. Invariably $\mathbf{R}_e \simeq -\frac{\nabla\cdot\mathbf{P}_e}{en_e}$. The expression above for δ_e using this approximation and dimensional analysis shows that $\delta_e \sim \frac{\rho_e}{L}$, where L is the scale perpendicular to **B** of the divergence and hence its contribution to $E_\perp$.

The size of δ_e constrains the size of the perpendicular part of Alfvén's violation of the *frozen in condition* relative to the size of B, viz

$$\frac{|\mathbf{R}_{e,\perp}|}{B} = \frac{w_{\perp,e}}{c}\delta_e = \frac{\lambda_{De}}{d_e}\delta_e. \tag{10}$$

At the forward magnetopause, $\frac{\lambda_{De}}{d_e} \approx .01$. and it provides the needed yardstick for the expected size of the perpendicular violation of Alfvén's *frozen in* condition: a small fraction of the size of B in cgs units. *Weak* perpendicular Alfvén *frozen in* violations are those where

$$|R_{e\perp}|_{weak} \ll \frac{w_{\perp,e}}{c}B, \tag{11}$$

while strong violations of the freezing in condition occur when

$$|R_{e\perp}|_{strong} \geq \frac{w_{\perp,e}}{c}B = 420\beta_e^{1/2}E_{recon}, \tag{12}$$

where $E_{recon} = 0.1\frac{V_A B}{c}$. If the reconnection electric field was or order $R_{recon} \approx 1\, mV/m$, this crossover between strong and weak violations would be accompanied by $R_e \approx 420\beta_e^{1/2}$ mV/m, which should be compared with much lower thresholds previously suggested experimentally.[15]

B. ϵ: Work per gyroperiod is small compared to kT

The second guiding center expansion perturbation parameter assumes that for each species, the average work done on all the particles per gyro period is small compared to the mean thermal energy

$$\epsilon_j \equiv \frac{2\pi|Z_j\mathbf{E}\cdot\mathbf{U}_j|}{kT_j\Omega_{ci}} = \frac{4\pi c}{w_{T,j}}\left|\frac{\mathbf{R}_j}{B}\cdot\mathbf{M}_j\right| \ll 1, \tag{13}$$

where $\mathbf{M}_j$ is the jth species thermal Mach number

$$\mathbf{M}_j \equiv \frac{\mathbf{U}_j}{w_{T,j}}, \tag{14}$$

where $m_j w_{T,j}^2 = 2kT_j$.

Specializing to the electrons, we establish a natural physical scale for violations of the total *non-ideal* electric field $\mathbf{R}_e$

$$|\mathbf{R}_e\cdot\hat{\mathbf{M}}_e|_{weak} \ll \frac{w_{T,e}}{4\pi M_e c}B, \tag{15}$$

and for substantial violations of the total *non-ideal* electric field,

$$|\mathbf{R}_e\cdot\hat{\mathbf{M}}_e|_{strong} \geq \frac{w_{T,e}}{4\pi M_e c}B, \tag{16}$$

where $\hat{}$ denotes a unit vector. The usually weak thermal Mach number of electrons $M_e \ll 1$ raises the size of the upper limit for weak violation of the non-ideal electric field; at the same time, the order unity $M_e \simeq 1$ typical of collisionless reconnection sites lowers the transition at which non-ideal $|\mathbf{R}_e|$ becomes strong and violating $\epsilon_e \ll 1$.

C. Relationships of δ_e and ϵ_e

With a little rearrangement,

$$\epsilon_e = \frac{4\pi w_{\perp,e}}{w_{T,e}}\delta_e\left(\hat{\mathbf{R}}_{\perp,\mathbf{e}}\cdot\mathbf{M}_{\perp,e} + \frac{R_{\parallel,e}}{R_{\perp,e}}M_{\parallel,e}\right), \tag{17}$$

showing that ϵ_e and δ_e are strongly correlated. The electron inertial scale of the current channel results in order unity electron thermal Mach numbers being a property of the separator regions of 2D layers (cf. Appendix E). As shown below, $M_{\perp,e} = \propto\delta_e$ yielding some regimes where $\epsilon_e \propto \delta_e^2$ when parallel Mach numbers are small. Violations of ϵ_e can also be stronger than for δ_e when electron parallel thermal mach numbers are significant. Equation (18) clarifies that large electron Mach number flows *can* make ϵ_e bigger than δ_e as does occur in the guide geometry.

D. τ_e: Reconnection rate and time variations are slow compared to gyro-period

The third premise of guiding center is that the time scale Δt of the variations in the system with frequency $\omega \simeq \frac{2\pi}{\Delta t}$ is slow compared to the respective gyro-period. Thus, the guiding center assumption is

$$\tau_j \equiv \frac{\omega}{\Omega_j} \ll 1. \tag{18}$$

A sense of the time scale precipitated by flux slippage at the separator may be estimated using Eqs. (2), (8), (11) to obtain

$$\nu_\Phi \sim \Upsilon \equiv \Omega_{ce}\delta_e^2 \simeq \Omega_{ce}A\emptyset_e, \tag{19}$$

where

$$\frac{c|R_{\perp,e}|}{w_{\perp,e}B} = \delta_e \simeq \frac{\rho_e}{L_{\nabla\times}} \tag{20}$$

has been used, with $L_{\nabla\times}$ assumed to be the spatial scale of the curl.

Accordingly, *at the separator*, the time variation expansion parameter *due to eroding flux* τ_e alone, would be estimated as

$$\tau_e \simeq \frac{\nu_\Phi}{\Omega_{ce}} = \delta_e^2 \simeq A\emptyset_e, \tag{21}$$

varying quadratically with δ_e or linearly with $A\emptyset_e$.

Equation (21) is the extension of Vasyliunas' theorem to three dimensions. From Eqs. (8), (16), (20), it is seen that (i) the misordering of one of the parameters accompanies misordering of others; (ii) that the regime $\delta_e \simeq 1$ produces a time variation via flux slippage that is non perturbative; (iii) $A\emptyset_e$ is a measure of the size of τ_e, as is δ_e^2, and (iv) the rate of magnetic slippage is $\nu_\Phi \sim \Omega_{ce}A\emptyset_e$, consistent with the insight of Vasyliunas' theorem.

E. Correlative signatures of electron demagnetization

In this section, we consider those state of the art observables that should accompany demagnetized electrons, with less extensive data inputs. The importance of these other diagnostics stems from their experimental independence from direct determinations of δ_e or ϵ_e or the electric field on which they depend; in this sense, they can be used in coincidence to guard against potential systematic effects in any given determination.

1. Electron thermal Mach number

Implicit in the demagnetization of electrons is that δ_e is finite, so that the scale lengths of the gradients in the problem are appreciable on the thermal gyroradius scale of the electrons. As the reconnecting magnetic field components reverse, there must be an intense current in a channel of scale $L \sim \rho_e$ as shown in Figure 7(a). As shown in Appendix E, Ampere's equation yields a *mean value* estimate for the component of the electron thermal Mach number orthogonal to the local plane of the reconnecting components to be

$$M_{e,z} > \delta_e \beta_e^{-1}(L) \frac{1}{\sqrt{1+S^2}}, \tag{22}$$

where β_e is determined in the total field at distance $x = L = \rho_e$ away from the field reversal point, and the guide field strength, S, is determined by $S = \frac{B_G}{B_R}$, the ratio of guide B_G to asymptotic reconnecting B_R components. The $>$ condition comes from the mean value character of the estimate, and for the ambiguity in the guide regime of there being two nested scales of current, one on ρ_e scale and another on d_e scale. As we show below in the symmetric case, the value of $\beta_{\perp,e}(L)$ in this region is often just below unity, so that M_e commonly approaches δ_e. In the strong guide regime, the scaling is apparently modified to be proportional to $\frac{BB_R}{8\pi nkT_e}$.

Since the electron *thermal* Mach number in ordinary MHD is commonly very low, the suggested variation of $M_{e,z} \uparrow O(1)$ in a diffusion region's current layer is a striking, and very unusual diagnostic, as we have recently demonstrated.[16]

2. Agyrotropy, $A\emptyset_e$

We have already mentioned that a model independent electron pressure tensor (from numerical quadrature) contains the information of the size of δ_e, since from[3,6]

$$A\emptyset_e \equiv 2\frac{|P_{e,\perp,1} - P_{e,\perp,2}|}{P_{e,\perp,1} + P_{e,\perp,2}} \sim \delta_e^2. \tag{23}$$

By measuring the velocity distribution function in an unaliased, model independent way in three dimensions, electron agyrotropy can be a correlative measure of demagnetization, without explicitly measuring electric fields required for δ_e.[16] This delta scaling has been recovered from the Polar Hydra measurements[18,19] and from PIC simulations[7] and constrains the Frobenius determinant of the irreducibly tensorial part of the pressure tensor.[20]

3. The angle between Eigen-vectors of $\mathbf{P_e}$, $\mathbf{E}_\perp$, α_e

Since the agyrotropy of Vasyliunas' theorem is required to be coherent when supporting the steady state reconnection electric field at the separator, it must be maintained by a coherent force that can put a "bulge" on the surface representation of the pressure tensor. Initial explorations[6] with PIC simulations have shown that indeed the perpendicular electric field seems to cause this bulge; this same effect has also been observed with 3D PIC simulations. The evidence for this effect involves the eigenvectors of the pressure tensor once the parallel pressure tensor contribution has been removed. This tensor T_{ij} is related to P_{ij} by the projection $\mathbf{T} = \mathbf{P_e} - (\hat{\mathbf{b}} \cdot \mathbf{P_e} \cdot \hat{\mathbf{b}})\hat{\mathbf{b}}\hat{\mathbf{b}}$. The effect that has been noted is that the minimum angle

$$\alpha_e \equiv a\cos(\hat{\mathbf{T}} \cdot \hat{\mathbf{E}}_\perp) \ll 20^\circ \tag{24}$$

between the eigenvectors of $\mathbf{T}$ and $\mathbf{E}_\perp$ does go through a distinct minimum, well below 22.5° in the presence of direct determinations of $A\emptyset$ or strong δ_e^2.[6] The 22.5° regime is the typical angle for this separation when the eigenvectors perpendicular to $\mathbf{B}$ are randomly chosen by the Gram-Schmidt orthogonalization program when their eigenvalues are computationally degenerate. When the scale of $\mathbf{E}_\perp$ is comparable to ρ_e, it can directly do work on the electrons. It can preferentially enhance their dispersion along $\hat{\mathbf{E}}_\perp$, breaking the cylindrical degeneracy of otherwise gyrotropic perpendicular eigenvalues. This effect is an important cross check on the direct determinations of $A\emptyset_e$, since its recovery depends sensitively on knowing $\mathbf{E}$ and accurately transforming the plasma observations into the electron fluid's rest frame. Errors in transforming to the electron rest frame can give a "phantom" signature of this type.

4. Anisotropy, An_e

While significant electron pressure anisotropy $An_e \equiv \frac{T_{\|e}}{\langle T_{\perp,e}\rangle} > 1$ is not directly a measure of demagnetization, it does occur in an *electron magnetized* regime of the ion diffusion region where parallel electric fields energize electrons in the parallel direction while the electrons cool transverse to $\mathbf{B}$ by moving into a weaker field regime. From PIC simulations, it has been noticed that unusual $An_e > 1$ is usually found *outside of, but juxtaposed to* the 2D separator on the low density side of the reconnection layer. These layers have also been seen with $An_e > 8$ during a recent *in situ* detection.[16] Orbit trajectories and other modeling within the PIC environment suggest that this anisotropy is created by electrons bouncing in a contracting mirror configuration while the magnetic field strength is weakening, but while the electron trajectories remain magnetized.[17] Such studies have shown electron $An_e \equiv T_\|/T_\perp$ range from 10 in PIC guide geometries to 2–3 in symmetric geometries. This effect is especially strong on asymmetric layers, where the low density side preferentially has the enhanced An_e and accentuated by low β_e. As soon as the plasma makes progress into the separator layer proper, the agents that demagnetize the thermal electrons cause the high An_e values to relax more towards isotropy, since the field is no longer an organizing agent.

This strong variation of An_e in the discovery transit[16] is particularly striking (shown in Figure 15, below). Since the expected values of An_e are *so atypical* for thermal electrons, their detection may be viewed as strong contextual confirmation of where the observer is located in the layer.

5. Convergent normal electric fields, E_n

The stagnation point flow of the steady reconnection pattern seems to require rather strong electric fields pointing into the diffusion region around the perimeter of its roughly elliptical outer boundary. At one level, such an electric field pattern may be *explained* as a "Hall" electric field caused by the strong electron out of plane drift, supporting the $M_{ez} = O(1)$ situation discussed above. However, such an explanation presumes that the electrons remain magnetized in this layer and they generally are not. As the guide field B_G becomes comparable to the reconnecting field component B_R, there is an additional term that may add or subtract from this E_n field associated with cross product of the exhaust velocity and the guide field. *If* these flows remain magnetized, the implied Hall electric fields along the normal E_n can be very strong compared to the reconnection electric field $E_R \simeq 0.1 \frac{V_{ai} B_R(\infty)}{c}$, with a startlingly strong ratio of

$$\frac{E_n(x)}{E_R} = 420 M_{e,R}(x) \frac{B_R(x)}{B_R(\infty)\beta_e(x)^{1/2}} \tag{25}$$

that reverses sign about the x point. If the exhaust speed is at the electron Alfvén speed in the strong guide field limit, it then becomes the dominant term in producing E_n. Because E_n contributions from the current contribution and that from the exhaust have different symmetries across the reconnection line, the ascendency of the one or other terms makes a big difference to the action of the electric field across the diffusion region.[21] The expected size of E_n will become smaller than the Hall estimated size when the flux slippage is acknowledged in the inner most regions of the current.

Up to modest guide fields comparable to reconnecting components, this slippage is allowed by enhancing $A\emptyset_e$, which in turn is caused by such large electric fields in gyroradius scale current channels. This may be the manner in which the growth of demagnetization limits the intensity of the converging E_n fields along the normal caused by the out of plane drift, and hence the magnitude of implied space charge build up.

6. Space charge density

Such a convergent electric field along the normal leads to an implied build up of negative space charge. However, the estimate of Eq. (24) relies on the electrons remaining magnetized and not slipping with respect to the magnetic field. The strong electric field will cause ϵ_e to grow and assist in the demagnetization of the electrons and $A\emptyset_e$ to increase, lessening the Hall electric field relative to the no slip prediction. Although routinely present in PIC simulations, the departure from charge neutrality is at present not measurable from spacecraft. Inferences of charge build up have been made using time sequences of electric field measurements, assuming they reflect spatial divergences. The size of the departure from quasi-neutrality seen in PIC is magnified relative to typical parameters in space by the typical simulation's adopted ratios of $\frac{\omega_{pe}}{\Omega_{ce}}$.

VI. FLUX SLIPPAGE, FLUX FUNCTION AND DEMAGNETIZATION IN 2D

A. Proxies vs Maxwell vs flux function in 2D

We now demonstrate in Figures 6 and 7 the especially clear way that proxies of demagnetization can identify the saddle point vicinity in 2d and the locales of "significant" flux slippage as determined by Λ_e. Figure 6 show quantities closest to those associated with the guiding center parameters, together with our proposed signatures of frozen flux slippage. Their colocation about the saddle point supports the perception that this layer is characterized by electron demagnetization. Figure 7 shows macro-variable corollaries of the demagnetization of the electrons.

Strong $O(1)$ enhancements of δ_e and ϵ_e are centered on the saddle point areas of the reconnection layer in insets 6(b) and 6(c); they clearly signal that guiding center approximation is misordered in these locales. Unlike the unobservable quantities in insets 6(a) and 6(e) which do have theoretical importance for frozen flux slippage, insets 6(b), 6(c), and 6(d) are all *observable* measures of the electron demagnetization. Agyrotropy, shown in inset 6(d), shows a two ribbon signature about the saddle point layer of this symmetric layer. The peak values in the ribbon are $A\emptyset_e \simeq 0.7$, while between these local maxima, a minimax occurs down to 0.3 on a line through the X-point (diamond in inset). The lateral spacing of the ribbon strands from this line through the X-point is approximately the turning point distance $x* = \sqrt{2d_e\rho_e}$ that is involved in the figure eight orbits about the X-line. The ribbons appear to be a non-local consequence of demagnetization in one locale intensified by trajectory effects away from the site of the demagnetization. This inference is supported by the black isocontour in this panel, whose inside contains $\delta_e > 1$ values. Contours superposed on the map of $A\emptyset_e$ illustrate the relationships between $\epsilon_e > 1$ and those for the composite $\kappa_e > 1$ which are all *between* the two ribbons of maximal $A\emptyset_e$.

The $\kappa_e = 1$ contours in panels (a)–(e) clearly show that there is no demagnetized electron regions outside of the highest enhancements of $\nu_\uparrow$, and there are no demagnetized electron regions outside the locale where $\Lambda_e \geq 1$. We thus see that the $\Lambda_e \geq 1$ and the violation of the proxy $\kappa_e \geq 1$ are mutually re-enforcing spatial signatures.

The spatial portraits for the dimensionless ancillary conditions in Figure 7 are "interesting" as proxies because their size reflects the demagnetization condition, even though an explicit determination of δ_e or ϵ_e is not required for their determination. In panels 7(a)–7(e), the cyan ellipse records the $\kappa_e = 1$ contour for reference: with the underlying color elevations of electron thermal Mach number, 7(a); departure from charge neutrality, 7(b); normal electric field E_x, 7(c), with overlaid white contours of $A\emptyset_e$; the minimum angle between perpendicular eigenvectors of $\mathbf{P}_e$ and $\mathbf{E}_\perp$, 7(d) also with overlaid white contours of $A\emptyset_e$; and, electron

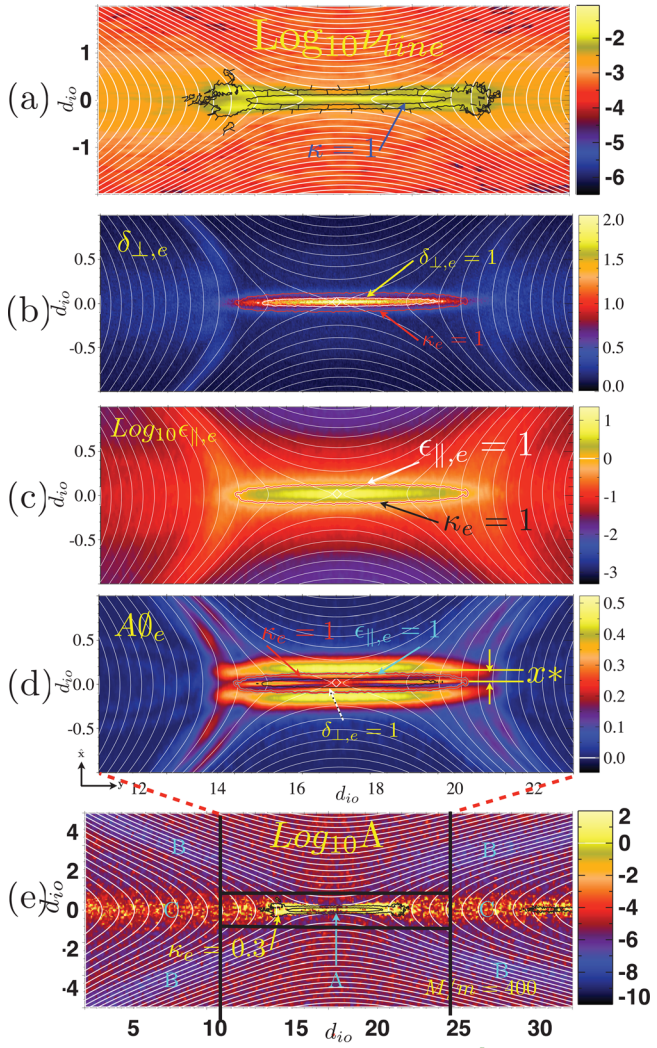

FIG. 6. (a) $\nu_{\uparrow}$; (b) $\delta_{\perp,e}$; (c) $\epsilon_{\|,e}$; (d) electron agyrotropy; (e) Λ_e. Simulation with M/m = 400 anti-parallel 2D PIC simulation.[13]

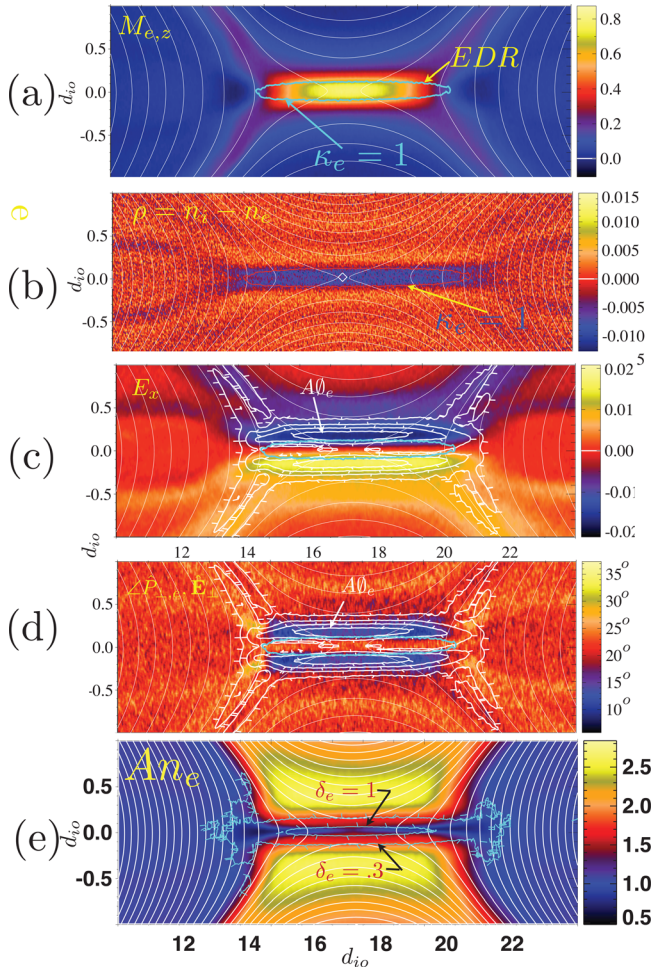

FIG. 7. (a) $M_{e,z}$ with contour overlay of $\kappa_e = 1$; (b) $\rho = n_i - n_e$, with contour overlay $\kappa_e = 1$; (c) E_x with overlay of $A\phi_e$; (d) smallest angle between eigenvectors of $\mathbf{P}_e$ and $\mathbf{E}_{\perp}$ with overlays of $A\phi_e$; (e) electron pressure anisotropy $An_e = \frac{T_{\|,e}}{\langle T_{\perp,e} \rangle}$. Same 2D PIC simulation as in Figure 6.

thermal anisotropy, (7e) with overlaid cyan contours of $\delta_e = 0.3, 1$.

Peak electron $M_{e,z} \geq 0.8$ correlates well within the $\kappa_e = 1$ contour and the $\nu_{\uparrow}$ enhancement of Figure 6(a), which is also the same region where $\Lambda_e \geq 1$ in Figure 6(e). The principle region of strong negative space charge in Figure 6(b) is also shown to occur within the $\kappa_e = 1$ contour, and by transitivity, with the others, including $\Lambda_e = 1$.

The normal electric field is strong where the peak of $A\phi_e$ occurs, arguing persuasively that the work done on the electrons by the intense normal electric fields plays an important role through $\epsilon_{\|,e}$, which is proportional to $\delta_{\perp,e}$, in creating $A\phi_e$. This latter conclusion is reinforced in Figure 6(d), where the minimum angle between the perpendicular eigenvectors of $\mathbf{P}_e$ and $\mathbf{E}_{\perp}$ has a pronounced minimum (below 22.5°) collocated within the maximum values of $A\phi_e$ indicated by the white overlaid contours.

Panel 7(e) provides the context about the EDR indicated in this figure by cyan contours of $\delta_{\perp,e} = 0.3, 1$, where it is clear that the enhanced "framing" anisotropy pattern is spatially complementary to the site of strong local demagnetization indicated by $\delta_{\perp,e}$. This enhancement is symmetric on both sides of the field reversal in this symmetric reconnection geometry. Wherever the electrons remain magnetized, such drifts produce an E_x directed towards the X-line from *both* sides. Since this field reverses sign, there must be net negative charge accumulation centered on the X-line as seen in Figure 7(b). There is an interesting interplay between producing ever stronger $\nabla \cdot \mathbf{E} < 0$ as the out of plane $U_{e,z}$ flow increases, which it does as the current channel narrows. So long as the electrons remain magnetized, stronger flows make larger E_x, so that their motion, carrying B out of the x-y plane also makes Hall contributions to E_x. We have seen that stronger $\mathbf{E}_{\perp}$ arising on short scales makes it possible to do more work on the electrons, even in the perpendicular direction, especially as they get demagnetized.

With increasing demagnetization, $A\phi_e$ increases, so does $\nu_{\uparrow} \sim \Omega_{ce}\delta_e{}^2$ and flux and electrons start to slip, reducing the normal electric field relative to what could have been made had they remain firmly magnetized. As a result of the converging E_x fields made by the Hall effect while the electrons remain magnetized, the space charge is negative and localized at the X-line. The strength of the space charge will be moderated as the very strong electric fields (of the Hall sense) do work on the electrons, increasing their agyrotropy,

enhancing slippage between electrons and magnetic field lines about the X-line. We speculate that the degree of agyrotropy growth for weak guide field geometries $S<1$ is a reflection of an attempt to minimize the net space charge of the X-line environs.

The correspondence of δ_e with $\nu_\uparrow$ in Figures 6(a) and 6(b) supports the suggested scaling of Eq. (20), while the depletion in $A\emptyset_e$ at the peak of $\nu_\uparrow$ seems to be a consequence of the moments over demagnetized orbits in this highly symmetrical reconnection model.

Figures 6 and 7 give a rather complete picture of our proxies for symmetric reconnection in 2D. When compared with a flux function, they bolster our certification that these proxies can find the X-point and its straddling non-ideal "diffusion region." However, *none of these pictures* can be provided from spacecraft measurements, even with the flotilla of satellites planned for the 2015 Magnetospheric Multi-Scale mission. Instead, such satellites collect data along world lines from which their analysis must be conducted.

B. Scales along width and breadth of the symmetric reconnection

The different scales of the anti-parallel reconnection solution of Figures 6 and 7 along the inflow and outflow axes are illustrated in Figures 8(a) and 8(b). Profiles are presented as a function of the integrated distance (in local electron inertial lengths) from the saddle point of the vector potential ($d_i = 20d_e$) of β_e, An_e, $A\emptyset_e$, n_e, $|M_{ez}|$, and κ_e provide an overview of the nesting of the highly structured EDR environs. Particularly clear is the demarcation in both panels of strong electron demagnetization within the vertical dashed lines where $\kappa_e \geq 1$ contours are traversed. Between these lines, gross departures from quasi-neutrality occur. Here, guiding center approximation expansion parameters summarized by κ_e are misordered, strong agyrotropy occurs, as anisotropy retreats from its enhanced values in the ion diffusion region (outside of the dashed lines) as the anti-parallel separator is approached, and as electron out of plane M_{ez} reaches its maximum. Above, we have shown this to be the locale of multiple signatures for broken line ($\nu_\uparrow \neq 0$) and topology ($\Lambda_e > 1$) of the magnetic field. The bottom panel demonstrates the extensive channel of electron demagnetization with $\kappa_e \geq 1$ of extent $\zeta > \pm d_i = 20d_e$ along the exhaust axis, which also contains high $\beta_e > 10$ during the most pronounced out of plane electron flows indicated by enhanced $|M_{z,e}|$.

The abrupt termination of the strong out of plane flows corresponds rather clearly to the retreating size of $\kappa_e < 1$, indicating a rather abrupt increase in the electron *magnetization* beyond the vertical dashed lines in both panels of Figure 8. From the point of view of strong demagnetization of the electrons, this strong decline of κ_e and $M_{z,e}$ provides an operational definition of the EDR's extent with one spacecraft scalar diagnostics. We have shown above the close correspondence between these diagnostics and $\nu_\uparrow$, Λ_e, A_z (cf. Figures 5 and 6); this is thus the region in which the magnetic field is being eroded at a hydromagnetically significant rate. *It should be considered a strong candidate for the magnetic dissipation region by virtue of these diagnostics and this chain of associations to the theoretical definitions.*

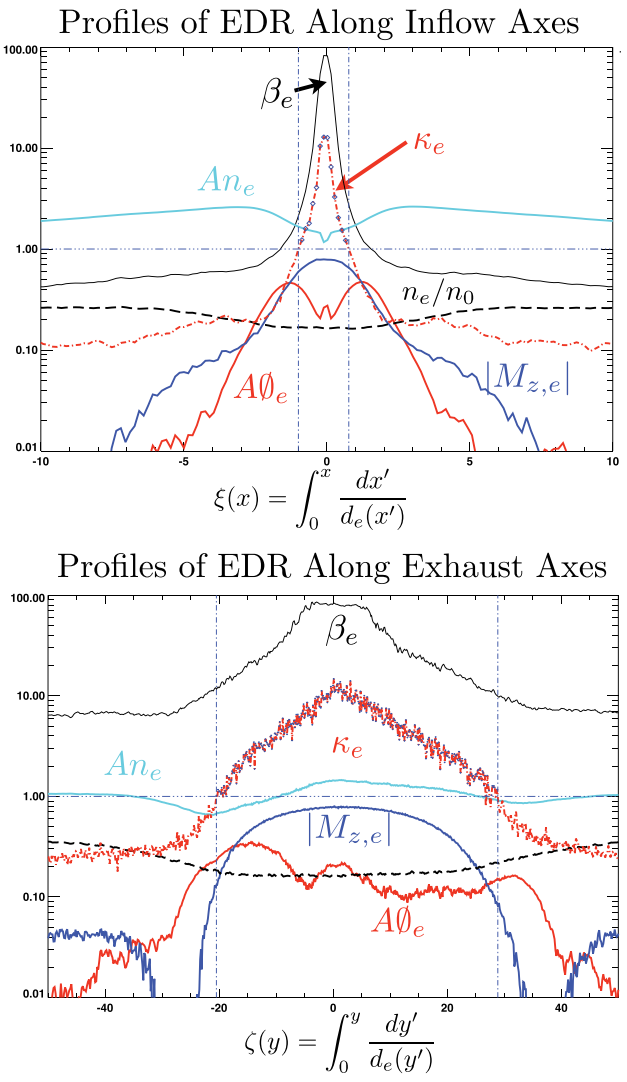

FIG. 8. Scales across (top) and along (bottom) the EDR of solution shown in Figures 6 and 7 using the proposed diagnostics, showing the organization of the layer, including thresholds and edge effects, where multiple, orchestrated signatures of electron *demagnetization* may be seen. The dashed lines in both panels denote the scalar condition $\kappa_e = 1$, suggesting the region $\kappa_e \geq 1$ is not guiding center ordered and the electrons are strongly demagnetized.

C. Magnetic diffusion $\Lambda_e < 1$ vs magnetic reconnection $\Lambda_e \gg 1$

In order to test our approach for differentiating magnetic *diffusion* from *reconnection*, a lower hybrid drift (LHD) unstable 2D PIC simulation was conducted with sheared magnetic fields along the simulation's symmetry Z direction, placing the current channel's variation in the simulation plane. In this geometry, the **k** vector for tearing growth cannot be supported, as it would require spatial variations along the Z axis. Thus, tearing reconnection is geometrically preempted. While this problem is *artificial*, it allows an important conceptual clarification of the thresholdless condition $\nu_\Phi > 0$ being a condition for diagnosing reconnection. We use this simulation to assess the calibration of our Λ_e

determinations as being consistent with our suggestion that $\Lambda_e < 1$ *with a threshold*, since here, it should indicate only anecdotal flux slippages where the flux function could confirm the topology.

The current channel in this simulation is so narrow that the cross field drifts are violently unstable to LHD instability. This causes the field lines to shuffle where they pierce the simulation plane, leaving a corrugated current channel in the x-y plane as shown in inset (c) of Figure 9 and also leaving a narrow $L \leq \delta_e$ scale current channel with large excursions of $A\emptyset_e > 1.1$, inset 9(d). As we have argued above, large $A\emptyset_e$ implies a substantial slippage $\nu_\Phi \simeq \Omega_{ce} A\emptyset_e$ of magnetic flux. Inset 9(a) shows there is indeed a noticeable enhancement in the flux slippage rate, $\nu_\uparrow$, along the current channel. Interestingly, our dimensionless rate parameter Λ_e in 9(b) is also enhanced along this channel. However, the histogram in 9(e) of *all* 32 768 determinations of $\Lambda_e(x, y)$ across the simulation plane clearly indicates that overwhelmingly $\Lambda_e(x, y) \leq 1$, and only very rarely (less than 0.01%) is Λ_e ever bigger than unity.

Eight circumscribing PIC cells of *each* PIC cell with $\Lambda_e > 1$ were examined for coincidence. Of these 10 noise cells with $\Lambda_e > 1$, only one had *an* additional noise spike in its eight circumscribing cells. Because of the log normal noise characteristics of Λ_e, it is likely that such low coincident rates are consistent with our surmisal that $\Lambda_e \leq 1$ is, in practice, a fair statistical summary of this simulation's properties. We refer to this regime as *"diffusion"* as its properties are similar to those of a weakly collisional current channel where one does obtain a slow diffusion equation for magnetic flux. This result, in conjunction with the much larger values of $\Lambda_e > 1$ illustrated in Figure 5 where flux functions in 2D confirm the reconnection site, restates the need for differentiating the weaker frozen flux violations from the stronger ones that the $\Lambda_e = 1$ line can provide. When flux functions are no longer available, this distinction can be of use with 3D simulations, and learning how to find reconnection layers in 3D from spacecraft.[7]

While the diffusion-reconnection distinction involving the size of $\nu_\uparrow$, ν_Φ, and $\Lambda_e \simeq 1$, boundary is theoretically useful, it is not fully differentiated by the size of the kinetic diagnostics like $A\emptyset_e$. Clearly, either regime requires non-zero $A\emptyset_e$. This makes $A\emptyset_e$ a *measurable* screen for either condition since agyrotropy is not routinely a part of the large scale plasma nor its normal modes. To observationally use $A\emptyset_e$ is to suggest that such a distinction requires additional considerations of geometry and inventories of hydrodynamic time scales and, in the best of circumstances, a supporting PIC simulation that makes predictions of sizes and spatial organization of their occurrence. Clearly, multi-spacecraft work can help with such arguments. For the present, it should be understood that this distinction needs to be argued for any given observational detection—at least until Λ_e becomes a routine observable, or has a quantifiable proxy that can differentiate its size.

If the plasma closures used in simulations *warrant*, we suggest that the computation of the size of Λ_e is useful for locating sites of reconnection in 3D simulations, where flux functions do not exist. As this example shows, the interpretations of significant $A\emptyset_e$ must consider the possibility that it may not be the separator region, but rather another area where there is significant flux slippage of the "diffusive" type where $\Lambda_e < 1$, such as we have shown above.

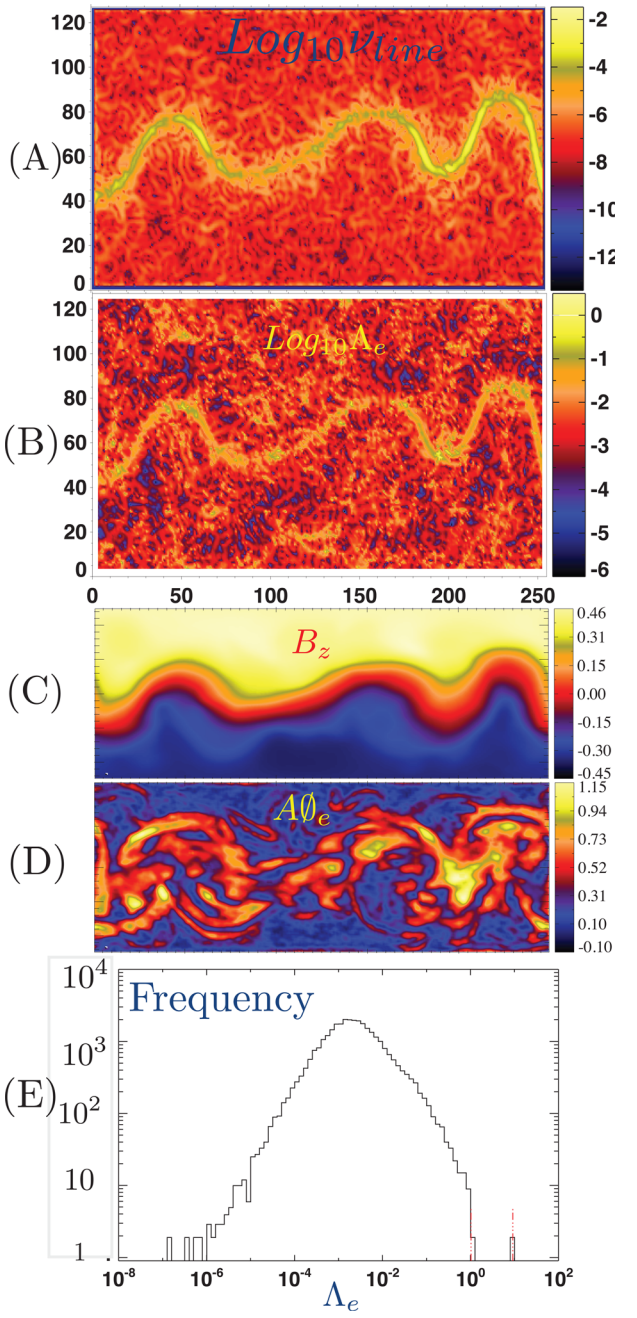

FIG. 9. (a) Rate of magnetic line slippage, $\nu_\uparrow(x, y)$; (b) dimensionless line slippage rate, $\Lambda_e(x, y)$; (c) out of plane $B_z(x, y)$ component of **B**; (d) electron agyrotropy $A\emptyset_e(x, y)$; (e) histogram of frequency across the grid of $\Lambda_e(x, y)$, showing overwhelmingly that Λ_e 1. Simulation performed using PIC code (Ref. 13) with mass ratio $M/m = 400$, with $\frac{w_{Te}}{c} = 0.236$, resolved by a 128×256 cells spanning 25×50 reference ion skin depths as indicated in panels (a) and (b). Panels (c) and (d) are vertical portions of the same horizontal regime, providing context of B_z and $A\emptyset_e$. Consistent with $\nu_\Phi \simeq (A\emptyset_e)$, there are strong enhancements of slippage and agyrotropy in these layers, despite their not possessing $\Lambda_e > 1$.

VII. DEMAGNETIZATION AND FLUX SLIPPAGE: 2D GUIDE GEOMETRY

A. Overview

We now focus on finding EDR transits with our proxies in the guide 2D geometry. This geometry has attracted considerable interest, since the guide field was thought of as a "magnetizing" force for the thermal electrons that would again establish electron magnetization and thus stall Collisionless Magnetic Reconnection (CMR). As we have outlined above, the essential aspects about magnetization of a species involve not only the ratio of the fields, $\frac{\mathbf{R}_{\perp,\|,e}}{B}$, but also the parallel and perpendicular thermal Mach numbers of the electron flow, $M_{\perp,\|,e}$. In addition, we will document the tendency for the increase in guide field to weaken the reconnection rate. Nonetheless, all the effects seen at the anti-parallel layer discussed above recur in the guide layers studied, but now, the misordering of guiding center approximation expansion parameters occurs preferentially in the energy change variable, ϵ_e, while systematic changes in the typical values of $\kappa_e(S)$ are indeed seen as the guide field strength S increases.

In the 2D guide geometry, the reconnection electric field is parallel to the magnetic field at the separator. Electron flows parallel to the guide field near the separator can be energized, making the guiding center approximation strongly misordered there via the energy change parameter, ϵ_e. This possibility helps to put $\epsilon_{\|,e} \gg \delta_{\perp,e}$ throughout the EDR. Counter intuitively, this places the responsibility for breaking's cylindrical symmetry prediction on the energy change per gyro-period condition, rather than disruption of $\delta_e \simeq \frac{\rho_e}{L} \ll 1$. Numerous independent PIC simulators[4] have reported the maintenance of the reconnection electric field at the 2D guide separator by the agyrotropic electrons. We show here that $\epsilon_{\|,e}$ is enhanced in the guide EDR, while δ_e (that hinges only on $R_{\perp,e}$) is smaller than in the anti-parallel geometry. This demonstrates that some of the expansion guiding center parameters remain significant while the more commonly discussed one is reduced in size with $\delta_{\perp,e} < 1$.

For the guide geometry, electron demagnetization in the form of $A\emptyset_e \neq 0$ does occur and labels the EDR about the saddle point. Vasyliunas's Theorem requires in 2D that $A\emptyset_e \neq 0$, but is silent about the requisite size of the expected violation. Simulations using the same PIC code[13] with open boundary conditions discussed above, but now with M/m = 360 show that the departures from gyrotropy are weaker in the guide geometry than in the anti-parallel geometry—a result that may not be so surprising since agyrotropy's role appears to facilitate adequate cross field electron mobility out of the plane. Because the guide component of **B** exists in the EDR and, the MHD reconnection electric field is a coherent $E_\|$ in this region, less demagnetization is required to facilitate the current to achieve the requisite short scales in this layer. We illustrate that trend below (Section VII D) with the variation of $A\emptyset_e$ with guide field strength, showing its systematic decrease with increasing guide field strength S over the range of $0 \leq S \leq 1.5$.

B. Guide domain of $\nu_\uparrow \neq 0$ and sizable κ_e

Initially, we focus on a symmetric guide geometry simulation with M/m = 360 and guide strength $S = 0.5$. Significant $\nu_\uparrow \neq 0$ extends ±5–6 local ion skin depths in Figure 10(a) on either side of the stagnation point and is within the "exhaust" zone *inside the preferred* magnetic separatrices (identified by flux functions which are in the 2nd and 4th quadrants about the separator. The overlying white curves of the magnetic topology demonstrate that this layer is within the exhaust side of the separatrix and not on, or straddling it nor astride X-points. This preferred separatrix layer is negatively charged. This charging is not peculiar to guide flux slippage layers, but a common feature seen in the anti-parallel geometry, where the flux slippage layer is more centrally confined. The deflection of the exhaust from horizontal is caused by the guide field's Lorentz force on the bulk velocity of the electrons. This produces a bias toward the preferred separatrix boundary, while the same forces and the weaker ion exhaust flows produce a weaker, but coherent initial ion deflection towards the opposite, unpreferred separatrix sheet in the same exhaust. This in plane polarization of charges supports the development of a secondary electric fields from separatrix to opposite separatrix in the x-y plane. Together with the guide field, this electric field ultimately pushes the increasingly magnetized plasma via $\mathbf{E} \times \mathbf{B}$ out the exhaust layer to form the final, more nearly neutralized exhaust moving with the ion Alfvén speed.

About the separator, a depression in $\nu_\uparrow$ is observed in Figure 10(a). Since the separator in the *symmetric* geometry is also a stagnation point, the curl of interest, $\nabla \times \mathbf{R}_e(\mathbf{x}_{stag}) \rightarrow \frac{\partial \mathbf{B}}{\partial t}|_{stag} \simeq 0$ in steady state. Thus, in a small, but finite neighborhood of the stagnation point, the integral for $\nu_\uparrow$ in steady state is expected to be locally depressed, even while nearby, outside of this $0.5d_i$ depression in the rate of slippage, $\nu_\uparrow$ is significant (as shown in Figure 10(a)). Within this region, the electrons out of plane Mach number, $A\emptyset_e$ and κ_e are enhanced in an especially localized way. In this layer, the reconnection electric field is wholly a parallel electric field and it strongly enhances $\epsilon_{\|,e}$ disrupting gyrotropy, and is the cause of the strong enhancement of $A\emptyset_e$ seen in Figure 10(e).

As discussed above, $\Lambda_\uparrow$ is the important dimensionless quantity for the hydromagnetic effectiveness of $\nu_\uparrow$; it contrasts the rate of flux slippage with inverse residence time in those conditions. The slow motion of the plasma immediately about the separator could elevate the fluid level importance of any finite $\nu_\uparrow$ there. Across the entire guide layer solution's red peak of $\nu_\uparrow$, the dimensionless $\Lambda_\uparrow$ exceeds unity over much of the exhaust layer *inside* the preferred separatrix (Figure 10(b)) although not reaching this level exactly at the separator for reasons discussed above. The greater than unity values of $\Lambda_\uparrow$ occur where $\nu_\uparrow \neq 0$, in the presence of large flow velocities that develop in the exhaust. The electron advection in this channel makes a large angle with the gradients of $\nu_\uparrow$, giving a protracted time for any finite rate of line disruption to have a cumulative effect on the hydromagnetics of the solution.

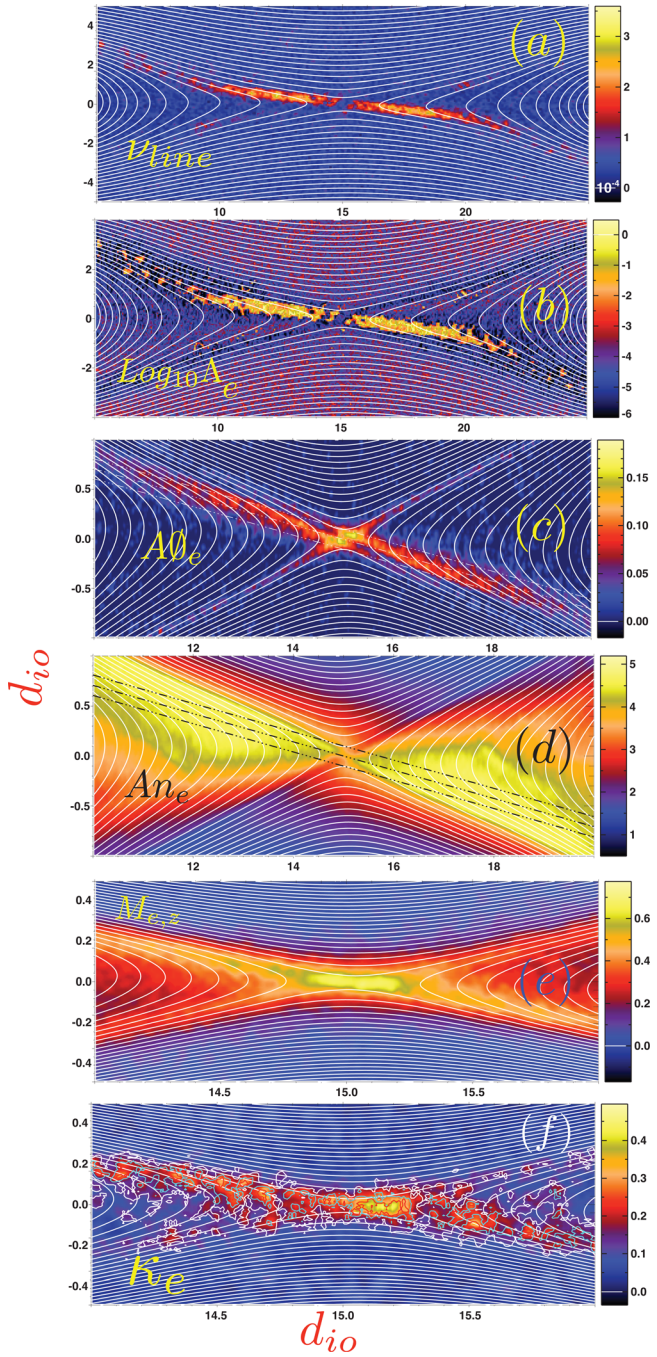

FIG. 10. 2D contours at symmetric guide field reconnection simulation with M/m = 360, with S = 0.5 (Ref. 13) of (a) $\nu_{\uparrow}/38$, (b) $\log_{10}\Lambda_e$, (c) $A\emptyset_e$, (d) An_e, (e) M_e, and (f) κ_e.

Just at the separator, the flows are weak, but aligned with the gradients of $\nu_{\uparrow}$ and $\Lambda_{\uparrow}(|s| \leq \frac{d_i}{2}) < 1$. As shown in more detail in Figure 10(b), the *hydromagnetic importance* of the loss of line labeling is briefly, but irregularly, depressed about the separator within a distance of $|s| < 0.5d_i$. The reduction in $\Lambda_{\uparrow}$ at the stagnation point is a reflection of the unduly symmetrical circumstance of these simulations that causes stagnation and magnetic X points to be superposed *and* slippage $\nu_{\uparrow}$ to also be reduced. In the more commonly occurring *asymmetric guide* geometry discussed below, these two points separate, and Λ_e remains high at the X point, as it is no longer the stagnation point.

Given the enhanced values of $\Lambda_e \leq 1$ along the preferred arms shown in Figure 10(b), and the preferentially enhanced values of $A\emptyset_e$ (Figure 10(c)) and κ_e (Figure 10(f)) along this arm, we identify the regions out to $\pm 4d_i$ in Figure 11(b) as the appropriate locale of *strong flux slippage* in this symmetric guide field layer. However, the vector potential contradicts that these are x-point locales, but are rather regions of intense, narrow currents, where there is none the less significant a magneto-hydrodynamically important magnetic flux slippage as part of the overall flow system about the reconnection site.

Along the topological separatrices (which are outside of the intense slippage arms), small $\nu_{\uparrow} \neq 0$ rates do occur, but are hydro-magnetically unimportant, since the sizable in-plane electron flows transit them quickly, these are more or less parallel to the gradients, yielding short transit times and $\Lambda_{\uparrow} \simeq 10^{-3} \ll 1$.

Thus, despite possessing intense electric fields and attendant agyrotropy (Figure 10(c)), the separatrices along all four extensions in both symmetric guide and anti-parallel geometry of reconnection are not sites of hydromagnetically significant disruptions of magnetic line labels in 2D. What frozen flux slippage is in evidence along the separatrices should be thought of as anecdotal, and not hydromagnetically important. It remains to be seen whether free access to 3D allows such layers, which are clearly non-ideal in 2D, but not able to reconnect, will do so in 3D.

C. Details of the frozen flux violating layers in guide geometry

Figure 11 highlights the properties of the guide flux slippage layer along and between the dashed lines through the slippage layer in the An_e (Figure 10(d)), showing the spatial variation of Λ_e together with inventories of other diagnostics. $An_e \simeq 5$ is uniformly large along this ridge with values of electron anisotropy that are unusually high value for space plasmas. Selecting the data within these two dotted lines allows statistics to be formed over $1d_{io}$ normal to the canted axis of the strongest flux slippage (between the extremes of the dashed lines in the anisotropy panel). This allows histograms to be formed along this ridge for the mean (black), *harmonic* mean (green), max (red), min (blue), and variances (black bar about mean) to be determined as a function of distance, s, along the guide flux slippage layer, on either side of the separator (s = 0). The right column of histograms in Figure 11 contains those critical parameters (closest to the guiding center parameters) whose spatial portraits were discussed in Figure 10.

As shown in Figures 11(a) and 11(b), the zone of hydromagnetic non-idealness ($\Lambda_e \leq 1$) has a rather sharply defined extent, falling by nearly a factor of 100 at $\pm 4d_i(s)$ cumulative distance from the separator. The ragged, but strong reduction in hydromagnetic non-idealness is centered within $\pm 0.5d_i(s)$ of the separator. *As shown by the black arithmetic and green harmonic averages, the enhanced Λ_e layer away from the guide separator nearly always had mean values below unity (indicated by the cyan dashed line)*; only the values involving the (red) maximum estimates of Λ_e in each

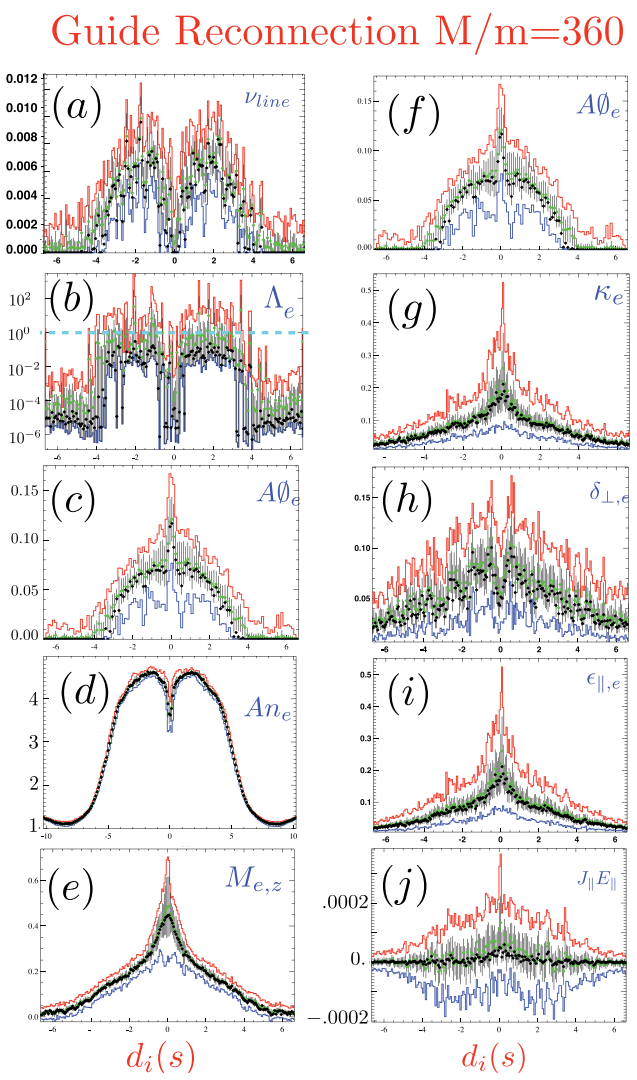

FIG. 11. Symmetric guide $B_z = 0.5B_y$.[13] Colors refer to harmonic (green), max(red), min(blue), variances (black bar) about mean (black dot), cf. text. Distance d is measured along the dotted line in Figure 10(d) in units of the *local* ion skin depth. Dashed cyan line in inset (b) is the cross over regime for $Lambda_e \simeq 1$ suggested by Eq. (7).

location show occasionally large values. The black variance bars (relative to the red traces) about the arithmetic mean confirm that the mean values *are* representative of the bulk of the measurements.

Consistent with our arguments concerning Eq. (7), Figure 2, and the flux function, these layers would not quantitatively be misconstrued as reconnection layers based on the Λ_e diagnostic. This is the second demonstration of the calibration of $\Lambda_e \simeq 1$ as an important dimensionless dividing line for anecdotal vs strong frozen flux violations. It is also known that the most unstable tearing modes in this geometry require wave vectors with components along the symmetry direction of the 2D simulation that are not allowed. In this sense, the slippage documented in Figures 10 and 11 is the residue of the closed exit channel for tearing mode growth.

As shown in Figures 11(c) and 11(f), the demagnetization (agyrotropy) attends the non-ideal exhaust current layer, and is systematically enhanced precisely astride the separator indicated by the flux function. Strong electron thermal anisotropies ($A_{ne} = 4 - 5$) are also seen throughout the flux slippage layer. However, from Figure 10(d), such high electron pressure anisotropies are a property of a larger volume in the exhaust (between separatrices) in which the principal flux slippage layers are immersed.

As in the anti-parallel case, that *entrance into the separator region is signaled by a strong enhancement of* $A\emptyset_e$ *accompanied by a local depression of* An_e *below the levels established outside in the ion diffusion regions*. The out of plane electron thermal Mach number is also enhanced along the entire slippage layer (Figure 11(e)). However, it has a shorter scaled maximum peak centered at the separator, where $\mathbf{E} = E_\parallel \hat{\mathbf{b}}$, at the depression of $\nu_\uparrow$ and Λ_e (seen in Figures 10(b) and 11(b)).

The right hand column of Figure 11 shows the spatial behavior along the flux slippage layer of the kinetic expansion parameters that are assumed infinitesimal in guiding center approximation. The composite $\kappa_e = \max\{\delta_{\perp,e}, \epsilon_e\}$ distribution shows the strong violation ($\kappa_e = 0.55$) at the separator, coincident with the strongly enhanced electron agyrotropy shown in Figure 11(f). A broad range of lesser κ_e violations along the length of the EDR are also seen. Unlike the anti-parallel case, here $\epsilon_e > \delta_\perp$ with the corollary that the central peak in $A\emptyset_e$ and κ_e reflects the misordered ϵ (energy gain per gyroperiod compared to kT_e). Unlike the regime where $E_\parallel \neq 0$ is the only way to have inordinate energy gain per gyroradius, significant energy gain occurs with the strong perpendicular electric fields in the presence of short scales as reflected in the agyrotropy profile.

The variation of $J_\parallel E_\parallel$ in Figure 11(f) is a factor (cf. Eq. (18)) in the size of $\epsilon_{\parallel,e}$, where the electrons are the dominant current carriers. It also has a large spike at the separator, where agyrotropy is strongly enhanced. $\epsilon \simeq 0.5$ signals a strong violation of adiabaticity and violation of the premises of expected gyrotropy. *In the guide geometry, agyrotropy is still found to support the reconnection process. It is seen to have a size in the guide geometry that scales more like* $A\emptyset_e \simeq \kappa_e^2$, *rather than the simple MacMahon result. However, the size of the agyrotropy seen is smaller than in an anti-parallel CMR geometry*. Vasyliunas' theorem is not contradicted by the weaker size of $A\emptyset_e$ nor the relatively weaker size of δ_e violations that occur, since ϵ_e violations compensate in disrupting expectations. Perhaps, more important is that demagnetization is an "assist" to help form cross field currents required. Since the reconnection electric field has a strong component parallel to **B**, the cross field current is less inhibited by the boundary conditions than in the anti-parallel case.

D. Demagnetization with increasing guide field strength

As there is a significant qualitative change between anti-parallel and guide (0.5) regimes, we summarize in this section a suite of symmetric simulations performed with all parameters constant, varying the guide field strength S between $0.05 < S < 1.5$. With increasing guide field strength, there is a strong and systematic decrease in the size of the

demagnetization parameters, κ_e, observed at the saddle point as shown in Figure 12(a).

This decrease is quantitatively brought together in Figure 12(b) and shown to be much stronger than the relatively weaker decrease in the rate of magnetic reconnection ($\frac{DA_z}{Dt}$) shown in red, even though the electron Mach number signatures (not shown) remained high as the guide field increased. Since the out of plane current is set by the size of the reconnecting (in-plane) magnetic fields (which are constant across these runs), the cross field current and thus Mach number should remain nearly constant as observed. This behavior is consistent with the view that $A\emptyset_e$ plays a prominent role enabling cross field current at low guide fields, but is less important for this purpose in the presence of the stronger guide fields that provide a relatively unencumbered out of plane current path. While the flux slippage is along the exhaust axis (not shown) for guide field strengths below 0.5, the flux slippage is preferentially found on the inflowing currents of the unpreferred axis coming into the separator region for guide field strengths above 0.5.

VIII. 2D ASYMMETRIC SIGNATURES OF DEMAGNETIZATION

Because of the general mismatches of density and field strength across the magnetopause, the current layer at the earth's magnetopause is generally asymmetric between the inflowing sides which have different magnetic field strengths and plasma pressures. In addition, the layer usually has a guide field that can be quite strong. The example shown in Figure 13 was produced from PIC code results,[13] with M/m = 100 and guide field of 0.5. Intersection of iso-contours where B_n (cyan) and B_z (yellow) vanish, was used to identify the separator. The stagnation point was identified from the flows to be above this intersection, but in front of the enhancement of agyrotropy indicated by the color relief contour. The green curve was a candidate trajectory considered to explain the recent resolution of the EDR by the Polar spacecraft.[16]

The implied size and phasing along the green curve of a subset of the proposed diagnostics of this paper from PIC are shown in Figure 14, and as measured by the GGS Polar spacecraft (Figure 15). The Polar data were reordered by the observed electron anisotropy, so that it is monotonic decreasing from its peak values on *either* side of the abrupt density transition seen in this asymmetric traversal. The reordering of the top panel of Figure 15 establishes the remapping for *all* other panels in the right column, so that they correspond to how anisotropy has been reordered in the top panel. The value of such a reordering has recently been shown using data from a 3D simulation to provide a similar clarification.[19] Clear coherent profiles of the expected size and ordering of $A\emptyset_e$, M_e, and even the strong electron heating (panel d) are thus observationally clearly demonstrated.

All five quantities of Figure 15 compared favorably in size *and* phasing with those suggested in Figure 14 from the 2D PIC simulations, lending further support to our thesis that our proxy diagnosis program can find the EDR in nature. On the basis of such detailed agreements, we have recently

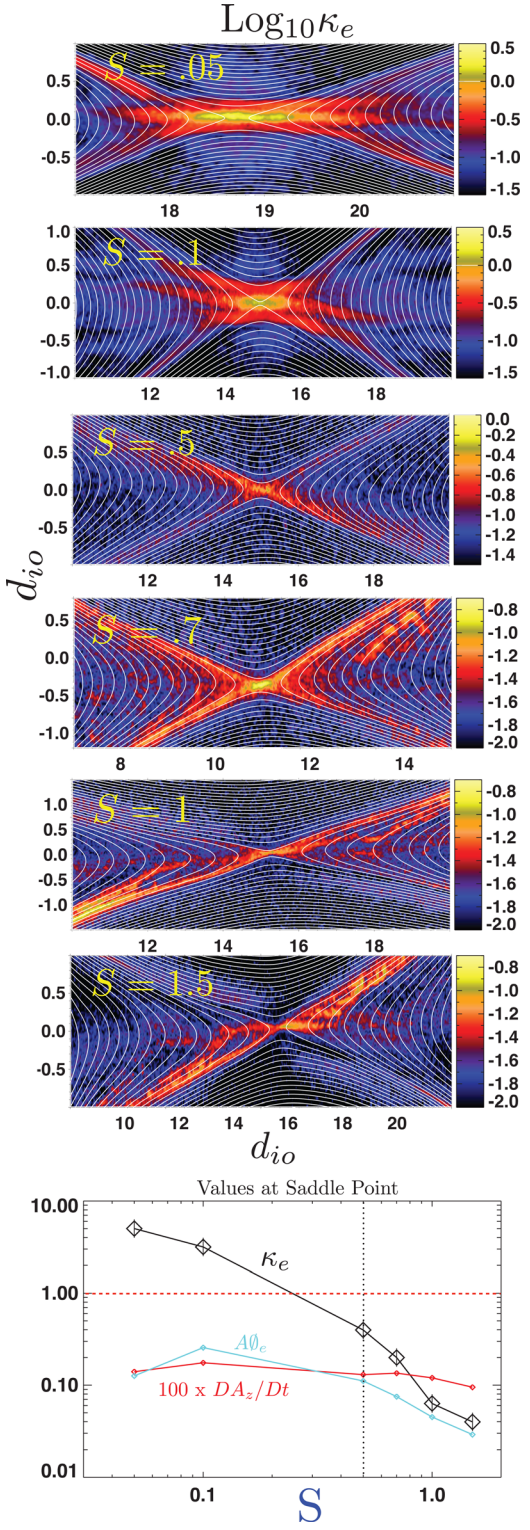

FIG. 12. (a) Variation of $\kappa_e(S)$ from symmetric PIC with guide strength S, M/m = 360;[13] (b) summary of demagnetization summary, agyrotropy, and reconnection rate vs guide strength S: $\kappa_e(S)$, $A0e(S)$, and $dA_z^{sp}/dt(S)$.

suggested this crossing as the first *resolved* traversal of the electron diffusion region.[16]

The large numerical values of the peaks of the dimensionless proxies in Figure 15 emphasize their "beacon" character when contrasted with other surveyed astrophysical plasma regimes: peak electron anisotropy in excess of 8;

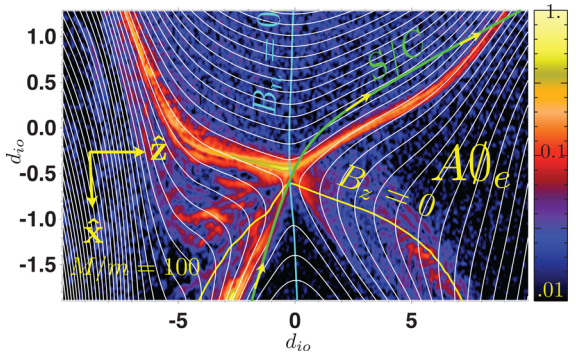

FIG. 13. $A\emptyset_e$ and magnetic geometry for 2D asymmetric, guide = 1, M/m = 100 simulation,[13] showing separation of the separator ($B_z = B_x = 0$) from the stagnation point, where agyrotropy is strongly enhanced. This figure also illustrates the contorted and deformed "X" near the singular points in the presence of strong asymmetry (density is lower on the upward side of the layer, while increased |**B**| on this side enables zeroth order pressure balance). The green line is the approximate trajectory of polar spacecraft for recently resolved EDR layer.[16] Underlying topography of $A\emptyset_e$ indicated by the color coded contour reveals more intense regimes of demagnetization on the low density side of the EDR. Reproduced from J. D. Scudder *et al.*, Phys. Rev. Lett. **108**, 225005 (2012). Copyright 2012 American Physical Society.

peak agyrotropy above 1.2; peak electron thermal Mach number > 1.8; direct signatures of bulk electron heating, nearly 150 eV above the higher of the asymptotic levels. There is no other known disturbance in space plasmas with these properties. Especially, persuasive is the observed electron thermal Mach number > 1.8, since even the supersonic solar wind only has an electron thermal mach number of $M_{e,SW} = 0.2$.

IX. DISCUSSION AND SUMMARY

At 2D reconnection sites modeled by PIC, we have shown that the relative size of electric and magnetic fields is misordered relative to the assumptions of guiding center approximation which is the underpinning of classical MHD. This misordering is strongest in anti-parallel geometry and weakened, but still present in anti-symmetric guide geometries with guide field strengths 1.5 times the reconnecting component. We have also shown with 2D PIC simulations

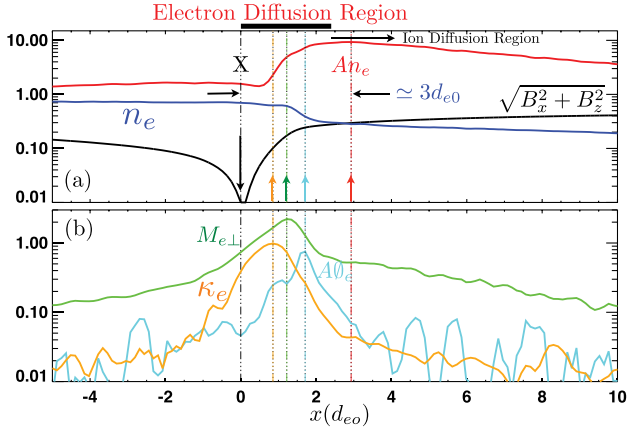

FIG. 14. Phasing of kinetic signatures[16] within asymmetric 2D PIC simulation of the EDR of Figure 13. Reproduced from J. D. Scudder *et al.*, Phys. Rev. Lett. **108**, 225005 (2012). Copyright 2012 American Physical Society.

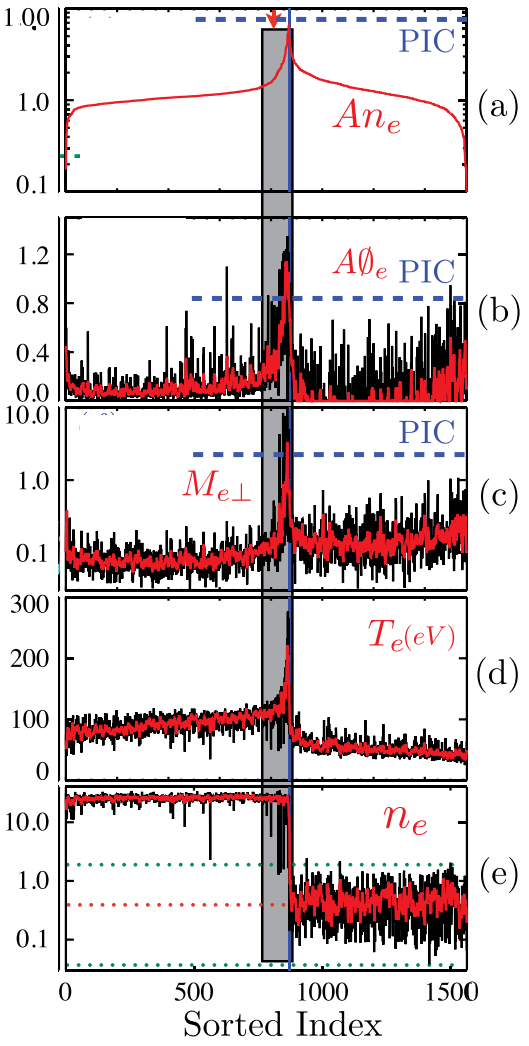

FIG. 15. Observed polar hydra kinetic signatures in first resolved electron diffusion region; sorting of data discussed in Ref. 16. The relative order and sizes of the demagnetizing signatures observed compare favorably with those from the PIC simulation reproduced in Figure 14. Adapted from J. D. Scudder *et al.*, Phys. Rev. Lett. **108**, 225005 (2012). Copyright 2012 American Physical Society.

that the domain inappropriate for the guiding center expansion corresponds well with the more mathematically defined sites of line and topology erosion based on $\Lambda_e > 1$ and the available flux function from A_z.

The EDR in symmetric anti-parallel and guide geometries possesses a coherent negative space charge throughout a macroscopic elliptic region about the separator; in the anti-parallel (guide) geometry, the semi-major to semi-minor aspect ratios o, this region is $2.1d_i$: d_e ($1.3d_i$: d_e) as determined from 2D anti-parallel simulations with mass ratios of 400 (360), respectively. Departures from charge density survive even at mass ratio $M/m = 1836$ and in 3D, but will be smaller for conditions in space where $\frac{\omega_{pe}}{\Omega_{ce}}$ is larger than can be presumed in the PIC simulations. In asymmetric 2D layers with guide fields, the negative space charge deforms and is found elongated along, but inside, the preferred sepatrix pairs, supporting additional ExB accelerations in the exhaust when coupled with the guide fields present.

Within the EDR we have illustrated a number of scalar, diagnostic, and observable proxies that help to find the regions of these intense scaled frozen flux violations in 2D simulations. Estimate of the size of these proxies make them atypically large for common properties in space plasmas. The values in the EDR of the proposed observable diagnostics are so atypically large relative to traditionally sampled astrophysical plasmas, that their calibrated detection (as opposed to any non-zero signatures) with space measurements are suggested to be invertible as to their cause (as we have recently done in asymmetric guide geometry[16]), and thus can act as viable *scalar* proxies screens for identification of the EDR. Our proposed rare kinetic proxies for the necessary frozen flux violation required in any formulation of the EDR are: (i) significant electron agyrotropy, $A\emptyset_e \simeq O(1)$, which can become O(0.1) when guide field strength is 1.5; (ii) non-negligible $\kappa_e = max\{\delta_{\perp,e}, \epsilon_e\} \simeq O(1)$; (iii) thresholds for sufficiently strong bipolar perpendicular electric fields of order 100 times the $0.1\,V_{Ai}$ inflow reconnection electric field for fast reconnection (cf. Eq. (24)); (iv) lower limit thresholds for what is meant by strong dimensionless parallel electric fields, sufficient to misorder the energy gain expansion parameter, ϵ_e (cf. Eq. (16)); (v) very large out of plane electron thermal mach number, $M_e \simeq O(1)$ (cf. Eq. (21)); (vi) enhancements of electron pressure anisotropy $An_e \geq 2$ within the innermost parts of the ion diffusion region for anti-parallel geometry and of order $An_e \geq 5$ or higher in, and surrounding, the electron jet exhaust up against the low density separatrix in the guide geometry's EDR layer; and (vii) coherent negative space charge density within the EDR proper. A common property of these proxies is that they are dimensionless, can be determined from a *single* spacecraft, and they involve properties *not* shared by other waves and discontinuities usually identified in hot magneto-fluid text books. As a screen their reliable observation implies rather unusual circumstances have been intercepted. The general scaling with guide field strength of these proxy violations of guiding center approximation requires more survey work with simulations.

The observable *disruption* of electron ordering parameters and their corollaries proposed in this paper involve comparing the *relative strengths of the non-ideal electric and magnetic fields and the electron Debye and skin depths*, cf. Eqs. (9) and (17). Properly, these are indices of the *particles and the fields* of the plasma state, not the fields alone, as has often attempted. When not in the reconnecting layers, the guiding center approximation predicts that these indices are perturbatively small relative to unity. *We have successfully argued that reconnection as simulated in 2D with PIC occurs where field and particles exchange momentum and relax their distorted fields enabled by the demagnetization of the electrons. The degree of this demagnetization is a function of guide field strength, an effect that needs more study.* It would be surprising if the collisionless reconnection site in nature could be convincingly identified only using center of momentum tests and successful Walén[24] tests alone—without an inventory that the plasma conditions are conducive to the demagnetization of the electrons necessary for loss of field line traceability through the layer.

Demagnetized electrons are not expected in large scale plasma, their normal modes, nor in the traditional MHD discontinuities that are dominated by ion demagnetization signatures. We have shown that observable signatures of demagnetized electrons can flag the locale of the EDR current layers and their separatrices that are unequivocally known from the details of the 2D PIC simulation. Accordingly, defensible detections of demagnetized electrons in the form of enhanced $A\emptyset_e$, κ_e, δ_e, ϵ_e of the threshold sizes mentioned above and/or extreme values of electron thermal Mach number M_e, or electron pressure anisotropy An_e could help with the evidence shortfall as to the cause of the current layers that are found in spacecraft data by the Walén test or in the **E** and **B** time series. Certainly, a flotilla of spacecraft can help with establishing the pattern of Walén like surfaces that attend any given "interesting" current layer chosen for study, or with the ensemble of single point characterizations of demagnetization signatures suggested here.

The new theoretical conditions proposed in this paper for the EDR involve antecedents and corollaries of $\nabla \times \mathbf{R}_e \neq 0$, while the usual conditions used for previous reconnection "detections" hinge on records of R_e different from 0. The evidence developed in this paper argues that the clear observable signatures of electron demagnetization involve the *scaled* size of R_e, since it controls the size of the guiding center parameters equations (8), (13), and (19). These signatures place thresholds on the necessary size of the dimensionless ratio $\frac{\mathbf{R}_e}{B}$ that controls the circumstances for demagnetization.

From the perspective of PIC simulations, the 2D diffusion region is a place where $\frac{R_e}{B}$ is so misordered relative to presumed ideal regimes of MHD that guiding center approximation ordering for thermal electrons is significantly and measurably disrupted there. The EDR is the result of the particles and fields organizing themselves about the stagnation point, with a non-neutral, negatively charged region as a corollary of the self consistent, broader flux slippage layer about the reconnection layer. *With this understanding the diagnostics for the EDR should be those that testify to these disrupted properties peculiar to the electrons, rather than center of mass fluid concepts, such as MHD wave velocities, jets, or patterns of* $\mathbf{E} \times \mathbf{B}$ *motions* that have some degeneracies with other normal modes of the plasma.

ACKNOWLEDGMENTS

We thank the referee for helpful comments. We gratefully acknowledge NSF Grant No. ATM 1153817, NASA NNX13AG08G, NASA Heliophysics Theory Program at LANL and SciberQuest. NSF has supported our calculations at Ranger and Kraken and NASA has supported this work through the High-End Computing (HEC) Program through the NASA Advanced Supercomputing (NAS) Division at Ames Research Center. J.S. acknowledges fruitful contacts with the MMS Science Team, editorial support from SED, and computer support from RDH at the University of Iowa.

APPENDIX A: ROLE OF $R_{EZ} \neq 0$ IN 2D FLUX SLIPPAGE

Maxwell's equation for the electric field equation in terms of the potentials takes the form

$$\mathbf{E} = -\nabla\phi - \frac{1}{c}\frac{\partial \mathbf{A}}{\partial t}. \tag{A1}$$

For the observer moving with the electrons, the partial derivative becomes an advective derivative and **E** transforms via Galilean relativity to yield

$$\left.\frac{d\mathbf{A}}{dt}\right|_{\mathbf{U}_e} = -c(\mathbf{R}_e + \nabla\phi). \tag{A2}$$

Since the gradient only has components in the (x-y) plane of the 2D simulation, the total time evolution of A_z is determined by the z component *alone* of the non-ideal electric field

$$\left.\frac{dA_z}{dt}\right|_{\mathbf{U}_e} = -c\mathbf{R}_{e,z}. \tag{A3}$$

Since the components of **B** in the x-y plane set the reconnection topology, and $B_x = \frac{\partial A_z}{\partial y}$ and $B_y = -\frac{\partial A_z}{\partial x}$, the time evolution in 2D of the reconnection topology is controlled only by the non-zero "out of plane component" of the violation of Alfven's "frozen in" condition. Thus, for example, while a parallel electric field makes $\mathbf{R}_e \neq 0$, unless $E_\parallel \hat{\mathbf{b}} \cdot \hat{\mathbf{z}} \neq 0$ its violation of Alfven's frozen in condition does not affect the slippage of flux in 2D.

APPENDIX B: A_Z AS 2D FLUX FUNCTION

A symmetry in 2-D simulations allows the out of plane component of the vector potential, A_z to be a flux function for the *instantaneous projections of the magnetic field into the x-y plane* where the gradients can occur. With these limitations, Ampere's equation implies

$$B_x = \frac{\partial A_z}{\partial y}, \tag{B1}$$

$$B_y = -\frac{\partial A_z}{\partial x}. \tag{B2}$$

The gradient of the scalar function $A_z(x, y)$ is the vector given by

$$\nabla A_z = \hat{\mathbf{x}}\frac{\partial A_z}{\partial x} + \hat{\mathbf{y}}\frac{\partial A_z}{\partial y}. \tag{B3}$$

These three equations imply

$$\mathbf{B} \cdot (\mathbf{I} - \hat{\mathbf{z}}\hat{\mathbf{z}}) \cdot \nabla A_z \equiv 0, \tag{B4}$$

which establishes that curves $(x(s, C), y(s, C))$ implicitly defined by $A_z(x(s, C), y(s, C)) = C$ are the projection of magnetic field lines in the *x–y* plane. These curves can easily be found by contouring $A_z(x, y)$ for a variety of contour values, C.

APPENDIX C: VASYLIUNAS' THEOREM

The argument in 2-D reconnection for the necessity of agyrotropy at the separator starts from the generalized Ohm's law. Near the stagnation point, the electron flow velocity goes to zero and the collisionless steady state electron momentum equations reduce to $\mathbf{E} = -\frac{\nabla\cdot\mathbf{P}_e}{en_e}$, with spatial variations only allowed in the x-y plane. The conserved reconnection electric is $E_z\hat{\mathbf{z}}$ and it must be supported by the electron pressure force. The electron pressure tensor must be tensorial to convert gradients in the x-y plane into a force along $\hat{\mathbf{z}}$. The next question Vasyliunas asked was whether an anisotropic, gyrotropic tensor could meet the needs of steady state. With a *reductio ad absurdum* argument, Vasyliunas showed this was not possible: the divergence of a gyrotropic tensor cannot provide the needed component of **E** at the stagnation point. Since tensorial electron pressure is the only possible way to get a $\hat{\mathbf{z}}$ component, the only remaining tensorial form that is not the gyrotropic tensor is the *agyrotropic* form with all symmetries broken. *Such an agyrotropic pressure tensor is the moment embodiment of substantial demagnetization of the electron velocity distribution function.*[3]

Vasyliunas's contradiction is developed by explicitly calculating the divergence of a gyrotropic tensor $\mathbb{P}_e$ organized by the local magnetic field direction $\hat{\mathbf{b}} = \frac{\mathbf{B}}{B}$, which can be written in general as[1]

$$\nabla\cdot\mathbb{P}_e = \nabla\mathbb{P}_{\perp,e} + \mathbb{S}(\hat{\mathbf{b}}\cdot\nabla)\hat{\mathbf{b}} + [-\mathbb{S}\hat{\mathbf{b}}\cdot\nabla lnB + \hat{\mathbf{b}}\cdot\nabla\mathbb{S}]\hat{\mathbf{b}}, \tag{C1}$$

where $\mathbb{S} \equiv \mathbb{P}_{\parallel,e} - \mathbb{P}_{\perp,e}$, and the eigenvalues are scalar functions. The gradients of these scalars functions in the 1st and 3rd terms of (A1) have no z components. Thus, any z components of Eq. (A1) depend on the behavior of $\hat{\mathbf{z}}\cdot\hat{\mathbf{n}}\frac{\partial}{\partial n}$. But $\hat{\mathbf{b}}\cdot\nabla \rightarrow \hat{\mathbf{b}}\cdot\hat{n}\frac{\partial}{\partial n}$ as the separator is approached, where $\hat{\mathbf{n}} = \pm\hat{\mathbf{x}}$ is a direction parallel to the inflow of plasma. The reconnecting, opposing components of **B** are solely in the $\pm\hat{\mathbf{y}}$ direction and approach zero at $x = 0$ at the separator. Below, we refer to their respective directions as $\hat{\mathbf{b}}_\leftrightarrow$. The Hall z components of **B** also approach zero in this limit as well. Even with a guide field, the directions of **B** remain steady as $\mathbf{B}_\leftrightarrow \rightarrow 0$. Thus, approaching the separator every term in (A1) vanishes as a consequence of the conditions below:

$$\mathbf{B}_{in} = lim_{q\rightarrow 0}\pm q\hat{\mathbf{y}} + B_G\hat{\mathbf{z}};\ \hat{\mathbf{n}} = \pm\hat{\mathbf{x}}, \tag{C2}$$

$$\hat{\mathbf{b}}_\leftrightarrow \Rightarrow \pm\hat{\mathbf{y}} \Rightarrow \hat{\mathbf{b}}_\leftrightarrow\cdot\hat{\mathbf{n}} = 0, \tag{C3}$$

$$\hat{\mathbf{b}}_g \Rightarrow \pm\hat{\mathbf{z}}; \Rightarrow \hat{\mathbf{b}}_g\cdot\hat{\mathbf{n}} = 0, \tag{C4}$$

$$\nabla_{in} = \mathbf{n}\frac{\partial}{\partial n} \Rightarrow \hat{\mathbf{b}}_{in}\cdot\hat{\mathbf{n}} = 0 \Rightarrow \hat{\mathbf{b}}\cdot\nabla_{in} = 0, \tag{C5}$$

$$\hat{\mathbf{z}}\cdot\hat{\mathbf{n}} \Rightarrow \hat{\mathbf{z}}\cdot\nabla_{in}\psi_k = 0. \tag{C6}$$

By contradicting the sufficiency of the gyrotropic approach, Vasyliunas concluded that steady CMR in 2D cannot be achieved within the gyrotropic closure approximation of guiding center approximation. As a last resort, the steady state EDR becomes a site of essential agyrotropy detectable in the electron pressure tensor, the testimony by the ambient electrons that they are *demagnetized*.

APPENDIX D: $A\emptyset_E$ IS PRESENTLY AN OBSERVABLE

Since Vasyliunas' theorem reflects a steady state pattern, the $A\emptyset_e$ constrained by his theorem is a time stationary pattern of the phase space density, and *not* the signature of gyro-

bunched electrons moving around at the electron cyclotron frequency. Such steady patterns of $\langle f(\mathbf{x},\mathbf{v},t)\rangle_t$ should be accessible to a plasma sensor that simultaneously *samples* differential fields of view $\Delta\Omega \simeq \sin\theta\Delta\theta\Delta\phi$ throughout 4π over the relevant electron energies in a time interval Δt short compared to the spacecraft rotation period, such that $\sqrt{\Delta\Omega} < \Omega_{S/C}\Delta t$. Such instruments have already been flown[22] and others have recently been launched on NASA's MMS mission.[23] The differences expected in the two perpendicular temperatures as a function of agyrotropy are measurable as has been shown previously.[6] Already at $A\emptyset_e = 0.1$, there will be a 10% difference in the two eigenvalues of P_e associated with eigenvectors perpendicular to $\hat{\mathbf{b}}$. The pressure eigenvalues are typically reproducible at better than 1%, so that such appreciable agyrotropies should be routinely measurable for a well calibrated detector.

APPENDIX E: $M_{EZ} \simeq 1$ HIGH ELECTRON THERMAL MACH NUMBER FLOWS EXPECTED IN EDR

The electron out of plane mach number is typically large when it supports a gyroradius scaled current channel as is expected within the EDR. Starting from steady state Ampere's equation, we have

$$\nabla \times \mathbf{B} = \frac{4\pi}{c}\mathbf{J}. \tag{E1}$$

Estimating the curl across the scale L and the change in **B** by $B_y(L) - B_y(-L)$, and approximating the current as supported only by electrons, we obtain

$$\frac{B_y(L)}{L} \simeq \frac{4\pi e n_e U_{ez}}{c}. \tag{E2}$$

Using

$$\frac{eB_y(L)}{mc}\frac{B}{B_y(L)} = \Omega_{ce} \tag{E3}$$

yields

$$M_{ez} \simeq \delta_{\perp,e}\beta_e^{-1}\frac{1}{\sqrt{1+S^2}}, \tag{E4}$$

where $L \simeq \rho_e/\delta_{\perp,e}$ and $S = \frac{B_z(L)}{B_y(L)}$ have been used.

APPENDIX F: EXPRESSIONS FOR δ AND ϵ IN PRESENCE OF AGYROTROPY

When averaged over an agyrotropic (tri-Maxwellian) distribution, $\delta_{\perp,e}$ and $\epsilon_{\parallel,e}$ have a slightly modified form

$$\delta_{\perp,e} \equiv \sqrt{\pi}\frac{cR_{\perp,e}}{w_{\perp,B}B}\left[\frac{2}{\pi}K\left(\frac{2A\emptyset_e}{2+A\emptyset_e}\right)\right], \tag{F1}$$

where $w_{\perp,B}$ is the larger of the two possibly different perpendicular thermal speeds. The energy gain parameter becomes

$$\epsilon_{\parallel,e} \equiv 4\pi\left|\gamma\delta_{\perp,e}\mathbf{M}_{\perp,\mathbf{e}}\cdot\hat{\mathbf{R}}_{\perp,\mathbf{e}} + \zeta M_{\parallel,e}\frac{E_\parallel}{B}\right|, \tag{F2}$$

with

$$\mathbf{M}_{\perp,e} \equiv \frac{\mathbf{U}_{\perp,e}}{w_{T,e}} \quad \text{and} \quad M_{\parallel,e} \equiv \frac{U_{\parallel,e}}{w_{T,e}}, \tag{F3}$$

where

$$\gamma = \frac{w_{\perp,B}^2}{\sqrt{\pi}w_T^2\left[\frac{2}{\pi}K\left(\frac{2A\emptyset_e}{2+A\emptyset_e}\right)\right]} \quad \text{and} \quad \zeta = \frac{w_\parallel d_e}{w_{T,e}\lambda_{De}}, \tag{F4}$$

where $K(x)$ is the first complete elliptic integral with $lim_{x\to 0}K(x) = 1$, and where $3mw_T^2 = 2Tr(k_B\mathbf{T})$.

[1]B. Rossi and S. Olbert, *Introduction to the Physics of Space* (McGraw-Hill, New York, 1970).
[2]V. M. Vasyliunas, Rev. Geophys. Space Phys. **13**, 303, doi:10.1029/RG013i001p00303 (1975).
[3]A. MacMahon, Phys. Fluids **8**(10), 1840 (1965).
[4]M. Hesse, K. Schindler, J. Birn, and M. Kuznetsova, Phys. Plasmas **6**, 1781 (1999); P. Pritchett, J. Geophys. Res. **106**, 3783 (2001); M. Hesse, M. Kuznetsova, and J. Birn, Phys. Plasmas **11**, 5387 (2004); P. Ricci, J. U. Brackbill, W. Daughton, and G. Lapenta, Phys. Plasmas **11**, 4102 (2004); L. Yin, W. Daughton, H. Karimabadi, B. J. Albright, K. J. Bowers, and J. Margulies, Phys. Rev. Lett. **101**, 125001 (2008).
[5]T. G. Northop, *Adiabatic Motion of Charged Particles* (Wiley, 1963).
[6]J. Scudder and W. Daughton, J. Geophys. Res. **113**, A06222 (2008).
[7]J. Scudder, *Magnetic Reconnection Concepts and Applications*, edited by W. Gonzalez and E. N. Parker (Springer-Verlag, 2016), Chap. 2.
[8]E. Priest and T. Forbes, *Magnetic Reconnection* (Cambridge Press, 2000); D. Biskamp, *Magnetic Reconnection in Plasmas* (Cambridge Press, 2000).
[9]J. Birn and E. Priest, *Reconnection of Magnetic Fields* (Cambridge, 2007); K. Schindler, *Physics of Space Plasma Activity* (Cambridge Press, 2000).
[10]F. S. Mozer, S. D. Bale, and T.-D. Phan, Phys. Rev. Lett. **89**, 015002 (2002); F. S. Mozer, S. D. Bale, T.-D. Phan, and J. A. Osborne, Phys. Rev. Lett. **91**, 245002 (2003); A. Vaivads, A. Retino, and M. Andre, Space Sci. Rev. **122**, 19 (2006); A. Retino, D. Sundkvist, A. Vaivads, F. S. Mozer, M. Andre, and C. J. Owen, Nat. Phys. **3**, 236 (2007); S. Bale and F. S. Mozer, Phys. Rev. Lett. **98**, 205001 (2007).
[11]G. Paschmann, Geophys. Res. Lett. **35**, L19109, doi:10.1029/2008GL035297 (2008).
[12]G. Paschmann, M. Oieroset, and T. D. Phan, Space Sci. Rev. **178**, 385–417 (2013).
[13]W. Daughton, J. Scudder, and H. Karimabadi, Phys. Plasmas **13**, 072101 (2006).
[14]R. D. Hazeltine and F. Waelbroeck, *The Framework of Plasma Physics* (Perseus, Reading, MA, 1999).
[15]F. S. Mozer, J. Geophys. Res. **110**, A12222, doi:10.1029/2005JA011258 (2005).
[16]J. D. Scudder, R. D. Holdaway, W. Daughton, H. Karimabadi, V. Roytershteyn, C. T. Russell, and J. Y. Lopez, Phys. Rev. Lett. **108**, 225005 (2012).
[17]J. Egedal, W. Daughton, and A. Le, Nat. Phys. **8**, 321–324 (2012).
[18]S. L. Rodriguez, J. D. Scudder, F. S. Mozer, and C. T. Russell, Fall AGU Meeting Abstract SM31A-1701 (2008).
[19]J. Y. Lopez, Ph.D. thesis, University of Iowa, 2015.
[20]N. Aunai, M. Hesse, and M. Kuznetsova, Phys. Plasmas **20**, 092903 (2013).
[21]Y.-H. Liu, W. Daughton, H. Karimabadi, H. Li, and S. P. Gary, Phys. Plasmas **21**, 022113 (2014).
[22]J. D. Scudder, F. Hunsaker, G. Miller, J. Lobell, T. Zawistowski, J. Keller, D. Chornay, F. Herrero, R. Fitzenreiter, D. Fairfield, J. Needell, D. Bodet, J. Googins, C. Kletzing, R. Torbert, J. Vandiver, R. Bentley, W. Fillius, C. McIlwain, E. Whipple, and A. Korth, Space Sci. Rev. **71**, 459–495 (1995).
[23]South West Research Institute, San Antonio, Burst Algorithm Definition and Concept Operation (BADCO) for the Magnetospheric MultiScale (MMS) Mission, May 2011, Document No 10160.17-BADCO-01, for contract NNG04EB99c.
[24]C. Walén, Ark. Mat., Astron. Fys. **30A**, 1–87 (1944).